Characterization of 2PA Chromophores

Eric W. Van Stryland and David J. Hagan

CREOL, The College of Optics and Photonics, University of Central Florida

4304 Scorpius Street, Orlando, Florida 32816-2700 USA

We review several experimental methodologies for the determination of nonlinear absorption coefficients of organic chromophores in either solution or thin film form. The goal here is to also be able to identify and quantify the nonlinear absorption process or processes, e.g. the essentially instantaneous two-photon absorption (2PA) or the cumulative excited-state absorption (ESA). These methods include the direct methods of nonlinear transmission and Z-Scan, along with the indirect methods of two-photon-induced fluorescence, excite–probe approaches, and Degenerate Four-Wave Mixing. We also discuss both frequency degenerate and frequency nondegenerate processes with emphasis on 2PA.

It is important to note that a single method is generally incapable of both measuring and identifying the source of the nonlinearity, thus it is usually necessary to employ more than a single method to determine the sign, magnitude and physical processes involved. For example, single beam experiments cannot give the temporal response of the nonlinearity while excite-probe methods do; however, single beam measurements lend themselves better to absolute calibration. In addition we include information on nonlinear refraction, which always accompanies nonlinear absorption processes. For example, the nondegenerate bound-electronic nonlinear refraction and ultrafast nondegenerate nonlinear absorption come from the real and imaginary parts of the nondegenerate third-order nonlinear susceptibility and are related by Kramers-Kronig relations via causality.

Keywords: nonlinear optics, absorption, refraction, organics, Z-scan, white-light continuum, structure-property relations, nonlinear photoacoustic/optoacoustic, thermal lensing, laser calorimetry, four-wave mixing, multiphoton ionization, excite-probe.

Table of Contents:

1. INTRODUCTION:

In this chapter, we describe several techniques for measuring nonlinear absorption (NLA) with special emphasis on the instantaneous nonlinear response of two-photon absorption (2PA)[1] due to its extensive use in microscopic imaging and 3D stereolithography/additive manufacturing.[2] We also give some information on nonlinear refraction (NLR) measurements since NLR almost always accompanies NLA signals. In general, multiple experimental techniques are needed to fully unravel the various physical processes involved in the nonlinear absorption for a given material, as it is rare to find only a single dominant nonlinear response. For example, 2PA not only causes a change in transmission but also results in the generation of excited states. These excited states can also change the absorption spectrum of the material which can easily be confused with the 2PA itself.

Additionally, NLR accompanies NLA and transforms into a spatial redistribution of energy upon propagation. Thus, in any experiment to monitor transmittance changes, considerable caution needs to be taken to ensure that the entire beam is collected by the detector for all input irradiances. Otherwise the NLR may be easily mistaken for NLA. Also, in order to be able to separate NLA and NLR, the conditions for external self-action, i.e., thin-sample approximation, need to be satisfied putting stringent requirements on the experimental parameters.[3] This will be discussed in more detail later. Even when NLA and NLR can be separated, obtaining reliable values for nonlinear coefficients can be difficult. For example, if the NLA is irradiance dependent (as for ultrafast nonlinearities) errors come from energy calibration (e.g. ±5%), temporal measurements (e.g. ±10%) and spatial energy distribution measurements (e.g. ±10% for Gaussian beams but for two dimensions). These errors add along with fitting errors (e.g. ±10%) to give an overall confidence error for the third-order nonlinear response. The example errors given in the previous sentence add to give a total error for the NLA or NLR coefficient of $\pm\sqrt{0.05^2+0.1^2+2\times0.1^2+0.1^2}=\pm21\%$. Measurement of higher-order responses would result in larger errors. All of these difficulties, as well as light simply missing the detector and incorrect identification of the physical processes, have led to reported values of nonlinear coefficients that vary over orders of magnitude from one publication to the next.[4-7] While such large discrepancies are becoming rarer due in part to more reliable, stable and well characterized optical sources and to our more complete understanding of the nonlinearities themselves along with the potential measurement problems, obtaining reliable coefficients with small confidence errors is still challenging.

2. DESCRIPTION OF NONLINEAR ABSORPTION AND REFRACTION PROCESSES:

2.1 2-Photon Absorption and bound-electronic nonlinear refraction

The second term after the linear optics term in Bloembergen's [8] expansion of the electric polarization

$$P \sim \varepsilon_0\left(\chi^{(1)}E+\chi^{(2)}E^2+\chi^{(3)}E^3+\ldots\right), \tag{1}$$

is the third-order polarization, which is characterized by the third-order nonlinear susceptibility $\chi^{(3)}$. This is the lowest-order term in the expansion that leads to "self-action" nonlinearities, i.e.

nonlinear absorption, which is proportional to the imaginary part of $\chi^{(3)}$ and nonlinear refraction proportional to the real part of $\chi^{(3)}$.

Assuming that the sample is thin in that the sample thickness is less than the Rayleigh length and the nonlinear phase does not propagate far enough to cause an irradiance change within the sample (i.e. external self-action[3]), the resulting equations for the propagation of the light irradiance I, and nonlinear phase shift φ, are:

$$\frac{dI(z,t)}{dz} = -\alpha I(z,t) - \alpha_2 I^2(z,t) \quad \text{and} \quad \frac{d\varphi(z,t)}{dz} = kn_2 I(z,t) \tag{2}$$

where z is the propagation distance, α is the linear absorption coefficient, α_2 is the two-photon absorption (2PA) coefficient, k is the wave number and n_2 is the nonlinear refractive index from $n=n_0+n_2 I$. Here, in MKS units, which are used throughout this chapter unless noted otherwise,

$$\alpha_2(\omega;\omega) = \frac{\omega\mu_0}{n_0}\,\mathrm{Im}\,\chi^{(3)}_{\mathrm{eff}} \quad \text{and} \quad n_2(\omega;\omega) = \frac{\mu_0 c}{2n_0^2}\,\mathrm{Re}\,\chi^{(3)}_{eff}, \tag{3}$$

where $\chi^{(3)}_{eff} = \frac{3}{2}\chi^{(3)}_{\Re,xxxx}(\omega;-\omega,\omega,\omega)$ for a single linear polarized input frequency of ω, where $E(z,t) = E_\omega \cos(kz-\omega t)$, and $E_\omega(z)$ is the slowly varying field amplitude with irradiance, $I = \frac{1}{2}c\varepsilon_0 n_0 |E_\omega|^2$.[9] We must mention here that this definition of α_2 in terms of $\mathrm{Im}\chi^{(3)}$ assumes that we are not within a region of linear loss where other effects, including absorption saturation would contribute. Equations 3 assume that the linear absorption $\alpha << 2\omega n_0/c$, otherwise α_2 becomes dependent on both the real and imaginary parts of $\chi^{(3)}$, as does n_2. This condition is normally satisfied except very near linear resonance.[10] For example, in the visible for an index of ~1.5 this becomes $\alpha << 2\times10^5$ cm^{-1}; however, for metallic nanoparticles, etc., this can be important.

The solution of Eq. 2 for the irradiance propagation is

$$I(L,t) = \frac{e^{-\alpha L}(1-R)^2 I(0,t)}{1+\alpha_2(1-R)I(0,t)L_{eff}}, \tag{4}$$

with $L_{\mathrm{eff}}=(1-e^{-\alpha L})/\alpha$ where L is the sample length, $I(0,t)$ is the irradiance incident on the sample, and R is the surface reflectance. If the thin sample approximation is not valid, amplitude and phase become intertwined with propagation within the sample and the full wave equation must be solved.[11] In the following sections we discuss specific methods for measuring the 2PA coefficient along with some complementary methods for determining n_2. NLR always occurs when α_2 is being measured, and sometimes it can be important. In addition, because 2PA and bound–electronic n_2 are related through Kramers-Kronig relations via causality, careful and complete measurements of nonlinear spectra can be used to derive spectra/dispersion of the other.

One should note that these Kramers-Kronig relations are strictly only valid for the frequency nondegenerate forms of the nonlinearities. [9]

When making measurements of organic dyes, solutions are often used since growing crystals can be very research intensive and making good optical quality solid-state films can also be difficult. In such measurements nonlinear cross sections are the more meaningful parameters to use. These cross sections are usually given in GM [12] units (1 GM = $1\text{x}10^{-50}$ cm^4s). For nonlinear absorption the cross section in terms of the 2PA coefficient is

$$\delta = \frac{\alpha_2 \hbar\omega}{N} \text{ , and } \delta_r = \frac{k_0 n_2 \hbar\omega}{N} \text{ ,} \tag{5}$$

where we have defined the NLR coefficient in an analogous fashion, with N the molecular density. The nonlinear coefficient per molecule may also be defined in terms of the second hyperpolarizability γ which is defined by:

$$\gamma = \frac{\varepsilon_0 \chi^{(3)}}{N f^4} \text{ ,} \tag{6}$$

where $f = (n^2 + 2)/3$ is the local field correction factor.[13] The molecular second hyperpolarizability is usually given in esu as $\gamma_{esu} = \frac{\chi^{(3)}_{esu}}{N_{cgs} f^4}$. For noninteracting solute and solvent molecules, assuming a nonabsorbing solvent, the nonlinear susceptibility of the solution is given by:

$$\left|\chi^{(3)}\right| = \frac{f^4}{\varepsilon_0}\left[\left(N_{solvent}\,\text{Re}\,\gamma_{solvent} + N\,\text{Re}\,\gamma\right)^2 + \left(N\,\text{Im}\,\gamma\right)^2\right]^{1/2} \tag{7}$$

where the index used in the local field correction factor is the index of the solution, i.e. solvent plus solute, and the γ's are the orientationally averaged molecular hyperpolarizabilities. If $N_{\text{solvent}}\,\gamma_{\text{solvent}} = -N_{\text{solute}}\,\gamma_{\text{solute}}$ (the contribution of the real parts due to solute and solvent cancel each other), the absolute value of $\chi^{(3)}$ of the solution has a minimum value given by:[14]

$$\left|\chi^{(3)}_{solution}\right|_{\min} = \varepsilon_0^{-1} f^4 N_{solute}\,\text{Im}\,\gamma_{solute} = \left|\text{Im}\,\chi^{(3)}_{solution}\right| . \tag{8}$$

This allows a separation and determination of the Re and Im parts of the nonlinear susceptibilities by varying the concentration to find the minimum.

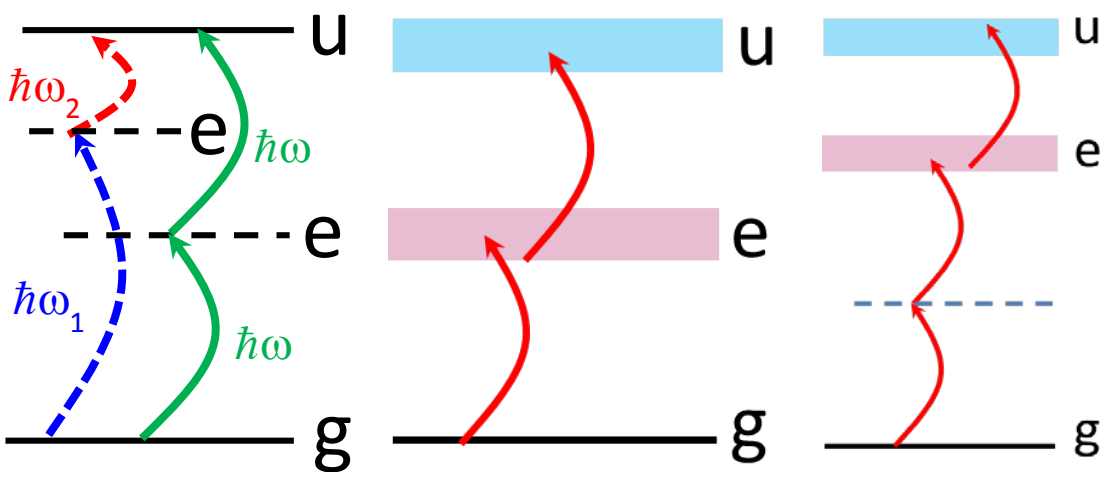

Figure 1. Left, Schematic energy–level diagram showing two-photon absorption from ground to excited state with equal photons (solid green lines) of energy $\hbar\omega$, or unequal photons (dotted blue and red lines) of energies $\hbar\omega_1$ and $\hbar\omega_2$ where $2\hbar\omega=\hbar\omega_1+\hbar\omega_2$. The dashed horizontal lines indicate what are commonly referred to as virtual states. Middle, resonant 2-step excitation of the upper state, u, with linear absorption cross sections between the states of σ_{ge} and σ_{eu} respectively. The rectangles are meant to indicate rovibronic transition absorption bands. Right, two-photon absorption to a band, e, followed by excited-state absorption to band u.

2.2 Excited-State Absorption and Refraction

The above description of 2PA and n_2 is strictly for bound-electronic nonlinearities which are ultrafast (sub-femtosecond). There are many other nonlinear responses which are pulsewidth dependent, and we describe just a few of these in the following. Many of these, such as excited-state nonlinearities, involve resonant, i.e. real absorption processes.[15] Organic dyes often display excited-state nonlinearities both in absorption, ESA, and in refraction, ESR. These effects are due to the redistribution of level/state populations. Figure 1 shows 'instantaneous' 2PA (left) where the intermediate off resonance state is labelled 'e' and the final upper state is 'u'. Transitions are 1-photon allowed from g to e and from e to u but not allowed by parity from g to u. It is instructive to look at the specific case of one-photon induced ESA in the case where saturation for the g to e transition is relatively small.[15] Figure 1 (middle) shows resonant 2PA, i.e., the intermediate state resonantly absorbs $\hbar\omega$ and is populated. The equations describing this phenomenon in terms of absorption cross sections, σ, are:

$$\frac{dI}{dz} = -\sigma_{ge}N_g I - \sigma_{eu}N_e I \quad \text{and} \quad \frac{dN_e}{dt} = \frac{\sigma_{ge}N_g I}{\hbar\omega}, \tag{9}$$

where N_g is the ground-state population density and N_e the population density of excited-state e in Fig. 1 middle, and the cross sections are between the labelled 1-photon allowed transitions. As the absorption has not been written in terms of a population difference we have included saturation of the linear absorption only as a ground-state depletion to low order, and we have assumed that once the excited state has been populated, it does not decay back to the ground state within the duration of the pulse. This is often a good approximation since the initial absorption in molecules is usually into a rovibronic band which rapidly relaxes to a lower energy from which ESA occurs, and this approximation is especially good when considering triplet states (not shown).

As 2PA and ESA are typically measured using short laser pulses, for which the measured quantities are the transmitted pulse energy or fluence (energy per unit area), we need to integrate Eqs. 9 over time. Under our approximations these two equations can be integrated over time to give a new propagation equation:

$$\frac{dF}{dz} = -\sigma_{ge} N_g F - \sigma_{ge} N_g \frac{\left(\sigma_{eu} - \sigma_{ge}\right)}{2\hbar\omega} F^2 , \tag{10}$$

where F is the time integrated irradiance or fluence, $F = \int_{-\infty}^{\infty} I(t)dt$.[15, 16] Equation 10 is good to second order in F. The last term, proportional to the square of σ_{ge}, comes from ground-state depletion which can sometimes be ignored as is true for the experimental case shown in Sec. 3.1.3. This equation is analogous to the equation for 2PA except that the fluence has replaced the irradiance and α_2 is replaced by products of one-photon cross sections. When performing perturbation theory to calculate two-photon absorption, it is the product of one-photon absorption matrix elements (proportional to the linear absorption cross sections) that enters the calculation. Thus this equation shows the transition from nonresonant 2PA to resonant, two-step, nonlinear absorption. There is a limited applicability of this solution as, for example, when the irradiance/fluence is increased, ground-state depletion becomes important.[16, 17] Looking at the similarity between Eq. 10 and Eq. 2, it is not surprising that this ESA has been mistaken for 2PA in some experiments. We show an example in Sec. 3.1.3. It is also the case that some authors define an effective 2PA coefficient to describe this ESA process; however, this coefficient is pulsewidth dependent while the true 2PA coefficient is independent of pulsewidth.

Associated with this ESA is ESR since a change in absorption also results in a change in index, both due to the redistribution of populations. The sign of the NLR will depend on the relative spectral positions of the resonances, i.e. above resonance or below. In this case the nonlinear phase shift is given by

$$\frac{d\phi(z,t)}{dz} = kn_2 I(z,t) + \left(\sigma_{euR} + \sigma_{geR}\right) N_e(z,t) , \tag{11}$$

where σ_{geR} and σ_{euR} are the nonlinear refractive cross sections for the ground and excited state respectively and we have kept the instantaneous NLR. Here the integration over time involves an averaging of the overall phase shift which results in a similar integral as for ESA which does not depend on pulse shape, giving an averaged phase shift of ½ the phase shift at the peak of the pulse,

$$\left.\frac{d\langle\phi(z,t)\rangle_t}{dz}\right|_{ESR} = \left(\sigma_{geR}+\sigma_{exR}\right)\frac{\alpha}{\hbar\omega}\frac{\int_{-\infty}^{\infty}dt\,I(z,t)\int_{-\infty}^{t}dt'I(z,t')}{\int_{-\infty}^{\infty}dt\,I(z,t)} = \frac{1}{2}\left(\sigma_{geR}+\sigma_{exR}\right)\frac{\alpha}{\hbar\omega}F \quad . \tag{12}$$

On the other hand, the instantaneous term gives an average phase shift that depends on pulse shape and is $1/\sqrt{2}$ for Gaussian temporal pulses, i.e.,

$$\left.\frac{d\langle\phi(z,t)\rangle_t}{dz}\right|_{n_2} = kn_2\frac{\int_{-\infty}^{\infty}dt\,I^2(z,t)}{\int_{-\infty}^{\infty}dt\,I(z,t)} = \frac{kn_2}{\sqrt{2}}F \quad . \tag{13}$$

Measurements of 2PA in semiconductors and many organic dyes are also accompanied by ESA but where the excited state is populated by 2PA. In this case, the irradiance propagation equation becomes,

$$\frac{dI(z,t)}{dz} = -\alpha I(z,t) - \alpha_2 I^2(z,t) - \sigma_{ex}N_e I \text{, with } \frac{dN_e}{dt} = \frac{\alpha_2 I^2}{2\hbar\omega} \tag{14}$$

as discussed in more detail in the experimental section where data is shown.

This is a higher–order process ($\mathrm{Im}\chi^{(3)}$:$\chi^{(1)}$), i.e. 2PA followed by linear absorption ($\mathrm{Im}\chi^{(1)}$), or 2PA followed by linear refraction ($\mathrm{Re}\chi^{(1)}$) as indicated in Fig. 1, right. Thus these are effectively fifth-order nonlinearities, so that this ESA can easily be confused with three-photon absorption (3PA), and many authors have defined effective 3PA coefficients, but again these will be pulsewidth dependent by necessity.[18] These nonlinearities are discussed in more detail in the sections describing specific experimental arrangements, e.g., Sec. 3.1.3 and 4.2.

The similarities of the propagation equations for ESA and 2PA as well as similar issues for higher-order nonlinearities present challenges for characterization techniques to uniquely determine the underlying physical processes. Unique determination often requires multiple methods and parametric studies, e.g. pulsewidth dependence. In the following sections we discuss several techniques for measuring these nonlinearities, the limitations of these methods, and possible combinations of methodologies to eliminate ambiguities.

3. METHODS FOR MEASUREMENTS OF NLA AND NLR

Measurements of NLA and NLR fall into two broad categories: *direct methods*, where we measure the self-induced change in transmission of a beam, and *indirect methods*, where an excitation is induced by a beam, to be sensed by some other means (transmittance of a probe, heating of materials, fluorescence, etc.)[19]

3.1 Direct Methods:

3.1.1 Nonlinear Transmission:

We start with perhaps the most straightforward and direct measurement of transmission as a function of irradiance. From Eq. 4, we find

$$\frac{1}{T}=\frac{I(0,t)}{I(L,t)}=\frac{e^{\alpha L}}{(1-R)^2}\left[1+\alpha_2 I(0,t)(1-R)L_{eff}\right] \tag{15}$$

where T is the transmittance.[20, 21] The equation is written in this way to point out a simple method for determining the 2PA coefficient by measuring the transmittance and plotting inverse transmittance versus irradiance. The result should be a straight line whose slope determines α_2 and intercept determines α. Of course, using Gaussian spatial and temporal profiles (or other shapes) requires integration over space and time These integrals reduce the slope for Gaussian shapes by a factor of $2\sqrt{2}$ (root 2 for each dimension of space and time), and for higher irradiance produces a downward curvature due to spatial and temporal beam reshaping, thus deviating from a simple straight line.[22]

Similarly for 3PA

$$\frac{1}{T^2}=\left[\frac{I(0,t)}{I(L,t)}\right]^2=\frac{e^{2\alpha L}}{(1-R)^4}\left(1+\alpha_3 I^2(0,t)(1-R)^2\left(\frac{1+e^{-2\alpha L}}{\alpha}\right)\right), \tag{16}$$

where it is assumed that there is no 2PA. Figure 2 shows a plot of inverse transmittance for a two-photon absorbing organic compound in thin-film form using femtosecond 810 nm pulses.[23]

Only the low irradiance inputs are plotted in Fig. 2 since at higher inputs 2-photon excited states linearly absorb leading to a higher-order nonlinear response. The slight upward turn as opposed to a slight downward curvature predicted due to the beam broadening by nonlinear absorption is due to this higher order process of 2-photon excited-state absorption. The straight line in Fig. 2 gives a slope which yields a value of $\alpha_2 \cong 30$ cm/GW which agrees with the values reported in Ref. [23].

While the experimental procedure appears to be simple and straightforward, one must beware of difficulties that result from the presence of nonlinear refraction in these experiments. If this nonlinear refraction is defocusing, it is quite easy for some of the beam to miss the detector at higher irradiances giving the appearance of a larger nonlinear loss. It is therefore not surprising that most inconsistencies in the literature involve reported values for the nonlinear coefficients being too large. It is also important that the detector response is spatially uniform. Additionally, as for any nonlinear measurement, the irradiance needs to be carefully calibrated necessitating measurements of the spatial profile as well as the temporal profile. Gaussian spatial profile beams are desirable since their propagation is particularly simple.

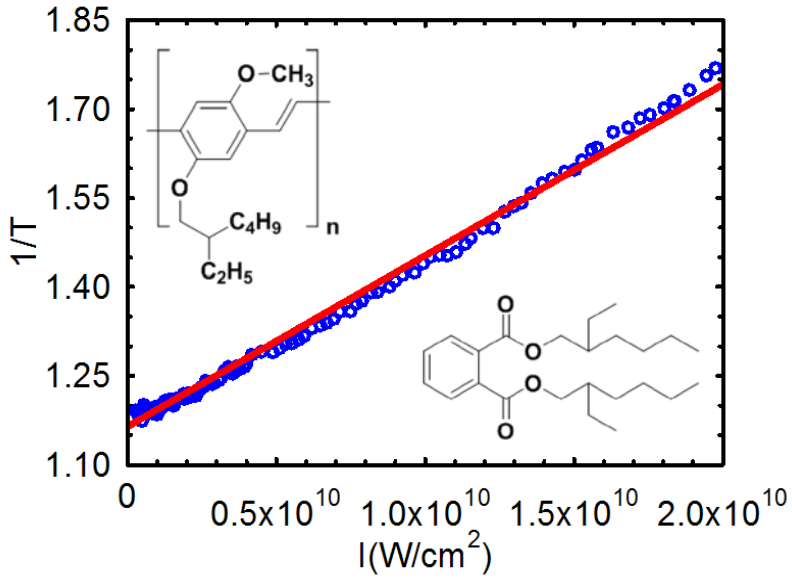

Figure 2. Data on a 25 micron thick film of MEH-PPV; DOP (50:50 melt-processed blend where DOP is di-octylphthalate, a plasticizer) as measured in Ref. [23], data provided by J. Hales, and replotted as inverse transmission versus irradiance. The upper left is MEH-PPV, and is lower right is DOP. The wavelength used was 810nm with 110 fs (FWHM) pulses.

The literature is filled with reports of high 2PA coefficients that are the result of either missing the beam due to nonlinear refraction or the use of pulses that have rapid temporal modulation that was not noticed.[22, 24] Similar problems can occur if the spatial profile is not smoothly varying at the sample. These comments can be applied to nearly all of the measurement techniques described in this chapter; however, there are ways to mitigate such problems, and many of these involve using known nonlinear samples as references or test samples.

Another comment about single beam direct transmission measurements that is self-evident is that they are sensitive to all nonlinear absorption processes and they do not differentiate between the different mechanisms that give rise to them; thus, other techniques must usually be used to determine the process or processes involved.

3.1.2 Z-scan:

Introduced in 1989, [25] the original Z-scan consists of translating a thin sample through the focus of a laser beam while monitoring the light transmitted through an aperture.[26] This gives a measure of the nonlinear refraction if there is no nonlinear absorption present. Gaussian spatial beams are preferred since modeling the results is greatly simplified, but not necessary. For measuring ultrafast nonlinearities pulsed sources are required and the signal is proportional to the temporally integrated nonlinearity. Figure 3 (left) shows the usual Z-scan setup for simultaneously performing open and closed aperture Z-scans, while (right) shows the configuration for a closed-aperture Z-scan where a reference arm is utilized to increase the signal-to-noise ratio, S/N.[27]

When nonlinear absorption is to be measured care is taken to open the aperture and collect all of the transmitted light. Typical signal profiles for Z-scans are shown in Fig. 4.

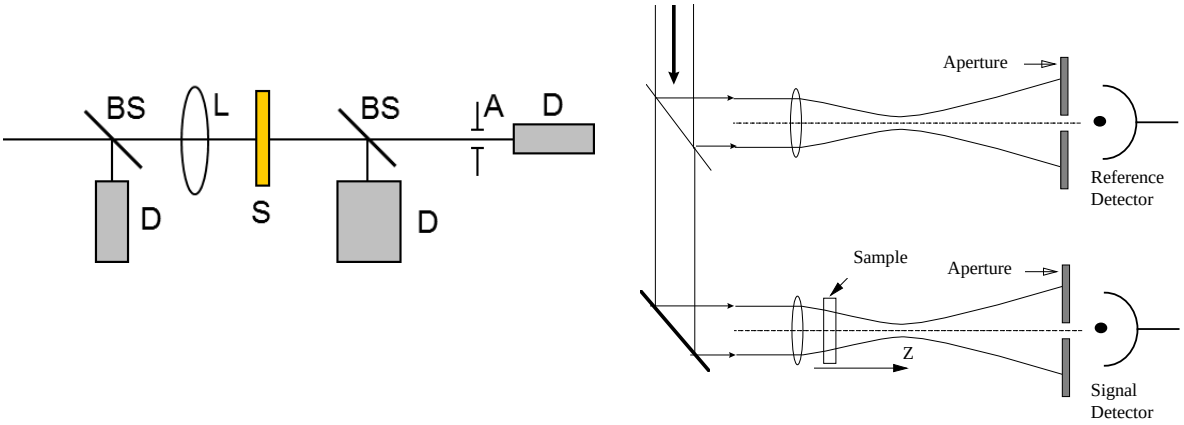

Figure 3. (Left) Z-scan setup allowing for simultaneous open and closed aperture Z-scans, (Right) Closed aperture Z-Scan with identical reference arm increasing the signal-to-noise ratio.[27]

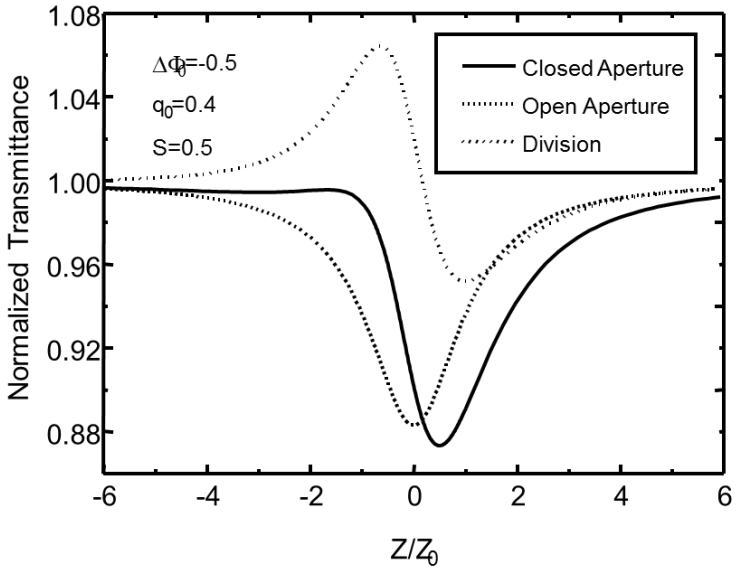

Figure 4. Calculated Z-scan signals using open, closed and divided signals as described for third-order nonlinearities (2PA and self-defocusing) with the parameters shown on the figure using the analysis described in Sec. 3.1.2.1 The separation of the transmission "peak" and "valley" for the divided signal is typically labelled ΔZ_{pv}, while the difference between peak and valley transmittances is commonly labelled ΔT_{pv}.

A beam splitter is often placed after the sample shown in Fig. 3 to split the transmitted beam onto two detectors. The first detector measures the total transmitted light, and is referred to as an open-aperture Z-scan. The second beam passes through the aperture in the far-field which typically transmits ~40% of the light in the linear regime which is collected onto a second detector. This is referred to as a closed-aperture Z-scan, i.e. partially closed. The open-aperture Z-scan is sensitive only to nonlinear absorption as long as the sample is thin as previously defined and the curve can be fit with a parameter describing the NLA (assuming there is a single NLA process!). The closed-aperture Z-scan is affected by both nonlinear refraction and absorption and given that the NLA has previously been fit, can be fit with a single parameter for the NLR (again under the assumption that there is a single NLR process!). However, if the closed-aperture signal is divided by the open-aperture signal the resulting curve is nearly identical to the signal that would have been obtained if the nonlinear absorption were absent - see Fig. 5. This can greatly simplify data analysis although the curve may also be fit with a 2-parameter fitting procedure for the nonlinear absorption and nonlinear refraction coefficients for third-order response materials, but with the usual increased errors associated with a 2-parameter fit. The popularity of the Z-scan technique is due in large part to the simplicity of separating absorptive and refractive nonlinearities; however, it is sensitive to ALL NLA and NLR mechanisms.

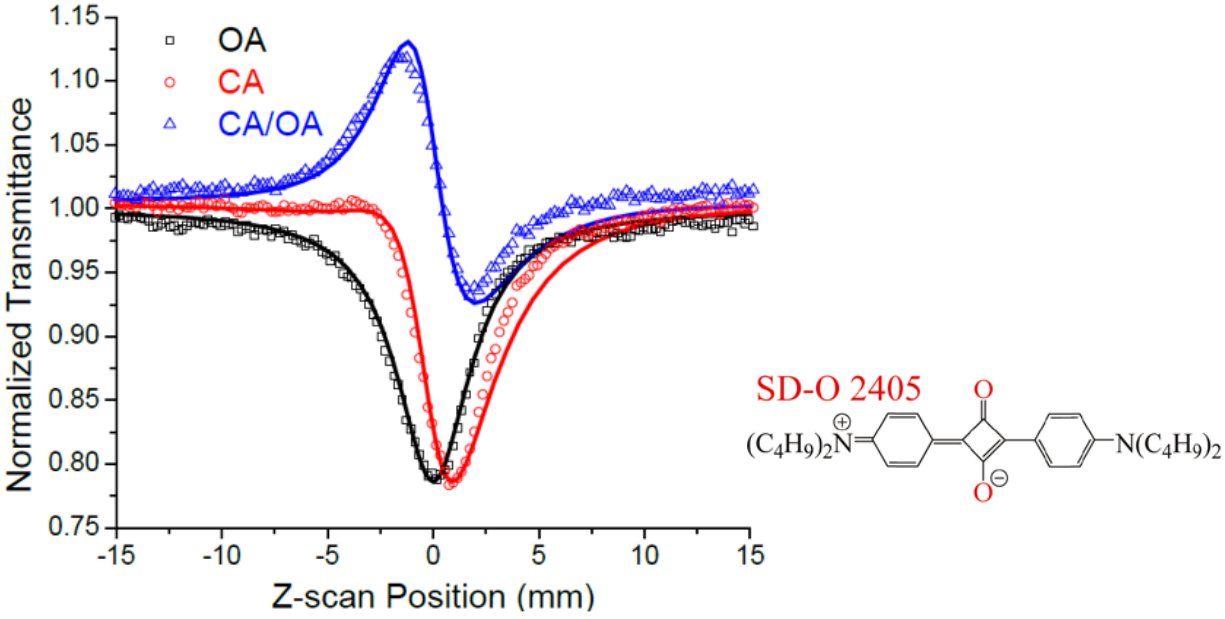

Figure 5. Z-scans, Open (black squares), Closed (red circles), Divided (blue triangles) for the squaraine molecule shown along with fits using only ultrafast α_2 and n_2.[28]

Shown in Figure 5 is an example of Z-scans (actually Dual-Arm Z-scans described in Sec. 3.1.2.2) using femtosecond pulses where only 2PA and n_2 are observed. The nonlinear refraction is from the solute only where the NLR from the solvent has been subtracted as described in Sec. 3.1.2.2. In the usual Z-scan, in order to determine the n_2 of the solute the NLR of the solvent must be subtracted by taking two sequential Z-scans, one with only the solvent and the other with the solution.

3.1.2.1 Simple Z-scan analysis:

A simple empirical relation exists between the peak to valley change in transmission measured in a Z-scan with Gaussian beams for the closed aperture Z-scan signal and the nonlinearly-induced phase distortion:[26]

$$\Delta T_{pv} \cong 0.406(1-S)^{0.27}\left|\Delta\Phi_0\right|, \tag{17}$$

where S is the linear transmittance of the aperture placed in the far field, and,

$$\Delta\Phi_0(t) = \frac{2\pi}{\lambda} n_2 I_0(t) L_{eff} \ , \tag{18}$$

where $I_0(t)$ is the an axis irradiance at focus and the effective length, $L_{eff} = (1-e^{-\alpha L})/\alpha$. This empirical relation is accurate for both cases without NLA and with NLA after division by the open-aperture Z-scan data. Since the temporally averaged transmittance is measured in a Z-scan, the pulse shape needs to be included. This is relatively straightforward given the linear relation between transmittance change and phase distortion of Eq. 17. If the irradiance dependent pulse shape in time is described by the function $f(t)$, then the temporal integral given by $A_\tau = \int_{-\infty}^{\infty} f^2(t)dt \Big/ \int_{-\infty}^{\infty} f(t)dt$, reduces the measured ΔT_{pv} by A_τ. This has the value of $1/\sqrt{2}$ for Gaussian pulses for nonlinearities much faster than the pulsewidth used. For pulses much shorter than the nonlinear response, e.g. excited-state nonlinearities, $A_\tau = 1/2$ independent of the pulse shape. In addition, the separation in Z between the position of the peak and valley is given by:

$$\left|\Delta Z_{pv}\right| \approx 1.71 Z_0 \, , \tag{19}$$

where $Z_0 = n\pi w_0^2/\lambda$, with w_0 the beam HW1/e^{2}M in irradiance. This allows an independent determination of the focused spot size if the sample is known to exhibit a third-order nonlinear response.

For the open aperture Z-scan, the peak energy transmittance change is given by:

$$\Delta T(Z) \approx -\frac{q_0}{2\sqrt{2}} \frac{1}{[1+Z^2/Z_0^2]}, \tag{20}$$

where $q_0 = \alpha_2 I_0(0) L_{eff}$ ($|q_0| << 1$). Here no propagation to the far field is required in the calculation since all energy is detected. The irradiance at the exit of the sample I_e is:

$$I_e(Z,r,t) = \frac{I(Z,r,t)\exp^{-\alpha L}}{1+q(Z,r,t)}, \tag{21}$$

while the phase change at the exit is:

$$\Delta\phi(Z,r,t) = \frac{kn_2}{\alpha_2}\ln[1+q(Z,r,t)], \tag{22}$$

where $q(Z,r,t)=\alpha_2 I(Z,r,t)L_{eff}$. This phase along with the irradiance distribution must be propagated to the detector in the far field to model the closed-aperture Z-scan data. There are multiple ways to perform this propagation and two of these are described in Ref. [26]. Thus, while the empirical results above are useful, the full propagation results can be fit for all Z which is good, for example, for checking the order of the nonlinearity. For example, a 3PA signal will be narrower in Z than a 2PA signal and $|\Delta Z_{pv}| \cong 1.5 Z_0$ for a fifth-order nonlinearity.

Combining Eqs. 21 and 22 we obtain the complex field at the exit surface of the sample to be

$$E_e(Z,r,t) = E(Z,r,t)e^{-\alpha L/2}(1+q(Z,r,t))^{(ikn_2/\alpha_2 - 1/2)} \quad , \tag{23}$$

while the field at the aperture is found by performing a Fresnel diffraction calculation:

$$E_a(\mathrm{Z,r,t,d}) = \frac{2\pi}{i\lambda\, d'}\exp\left(\frac{i\pi r^2}{\lambda\, d'}\right)\int_0^\infty r'dr'\, \mathrm{E_e(Z,r',t - d'/c)}\exp\left(\frac{\mathrm{i}\pi\, \mathrm{r'^2}}{\lambda\ \mathrm{d'}}\right)\mathrm{J_0}\left(\frac{2\pi\, \mathrm{rr'}}{\lambda\, \mathrm{d'}}\right), \tag{24}$$

where $d'=d-Z$ is the distance from the sample to the aperture plane. The measured quantity is the pulse energy or average power transmitted through the far-field aperture having a radius of r_a. The normalized transmittance is then obtained as:

$$T(Z) = \frac{\int_{-\infty}^{\infty} dt \int_0^{r_a} |\, E_a(Z,r,t,d)\,|^2\ rdr}{U}, \tag{25}$$

where U is the same as the numerator but in the linear regime (i.e. for $\Delta\phi = 0$). In the case of an EZ-scan, the limits of the spatial integral in Eq. 25 must be replaced by r_d to ∞ where r_d is the radius of the obscuration disk.[29, 30] It is generally more convenient to represent the aperture (or disk) size by the normalized transmittance (or rejection) S in the linear regime.

The formalism thus far presented is generally applicable to any radially symmetric beam. Here, however, we assume a $\mathrm{TEM}_{0,0}$ Gaussian distribution for the incident beam as given by:

$$E(Z,r,t) = E_0(t)\frac{w_0}{w(Z)}\exp\left(-\frac{r^2}{w^2(Z)} + i\frac{\pi r^2}{\lambda R(Z)} + i\phi\right), \tag{26}$$

where $w(Z)=w_0(1+Z^2/Z_0^2)^{1/2}$ and $R(Z)= Z+Z_0^2/Z$. The radially invariant phase terms, contained in ϕ, are immaterial to our calculations and hence will be ignored.

The integral in Eq. 24 can be analytically evaluated if we assume that $|q|<1$ (in Eq. 23) and then perform a binomial series expansion of E_e in powers of q. Recalling that $q \propto I \propto \exp(-r^2/w^2)$, this expansion effectively decomposes E_e into a sum of Gaussian beams with varying beam parameters. This method of beam propagation known as Gaussian decomposition was first given by Weaire et. al.[31] Following the expansion, we obtain:

$$E_e = E(Z,r,t)e^{-\alpha L/2}\sum_{m=0}^{\infty} F_m \exp(2mr^2/w^2(Z)), \tag{27}$$

where F_m, the factor containing the nonlinear optical coefficients, is given by:

$$F_m = \frac{(i\Delta\phi_0(Z,t))^m}{m!}\prod_{j=1}^{m}\left[1+i\left(j-\frac{1}{2}\right)\frac{\lambda\beta}{2\pi n_2}\right]. \quad (28)$$

Remarkably this single beam technique has a demonstrated sensitivity to induced phase distortion of $\sim\lambda/10^3$ while a simple variation, the "EZ-scan", which replaces the aperture with a stop, has a demonstrated sensitivity to $\lambda/10^4$.[29] There have been multiple other modifications of the basic Z-scan reported in the literature [27, 32-36]. This interferometric-like sensitivity comes about by the sample serving as a phase mask, which upon propagation to the far field is transformed into a spatial amplitude redistribution, i.e. via diffraction. That is, diffraction is an interference phenomenon between the wings of the beam which are weak and propagate nearly linearly and the center of the beam which undergoes a nonlinear phase shift, either advanced as for self-defocussing (n_2<0), or delayed as for self-focusing (n_2>0). Thus, the Z-scan serves as a single beam interference technique without the alignment complexities of interferometers.

3.1.2.2 Dual Arm Z-scan

Shown in Figure 5 is an example of Z-scans where only 2PA and n_2 are observed. Most, solvents do not exhibit 2PA in the visible or near infrared, so any observed 2PA can be attributed to the solute. However, the same is not true of NLR, and any measured nonlinear refraction comes from a combination of the NLR of the solvent and solute. In order to determine the n_2 of the solute, the NLR of the solvent must be subtracted. Since sometimes the solubility of molecules is limited, the solvent n_2 can overwhelm the solute NLR and make its determination problematic. One method to alleviate this problem is the "Dual-Arm" (DA) Z-scan [28] described below.

In the DA Z-scan (experiment shown in Fig. 6), a second Z-scan arm is arranged to have an identical optical path to that of the first arm. When initially aligned with identical cuvettes and the same solvent in each arm, the signal, which is the subtraction of the signals from each arm, can be nulled. When the solute is added to one arm, the resultant difference signal is then only due to the solute. In practice we find that this increases the signal-to-noise for NLR by a factor of ~10x (see Figure 7 of a squaraine molecule showing the increased S/N). The S/N increase for NLA is less dramatic. This increase in S/N for NLR comes about because much of the noise in each arm is correlated on each laser firing. This noise is effectively subtracted on each laser shot. For example, since closed–aperture Z-scans are sensitive to beam pointing instabilities, the dual arms provide an excellent way to reduce their effect since both arms move synchronously thus giving the same change in signal from this beam movement. This technique also works well for thin film samples on substrates to subtract the substrate signal and correlated noise.[37] Figure 7 shows the effectiveness of using this method for a squaraine dye in toluene showing both NLA and NLR.

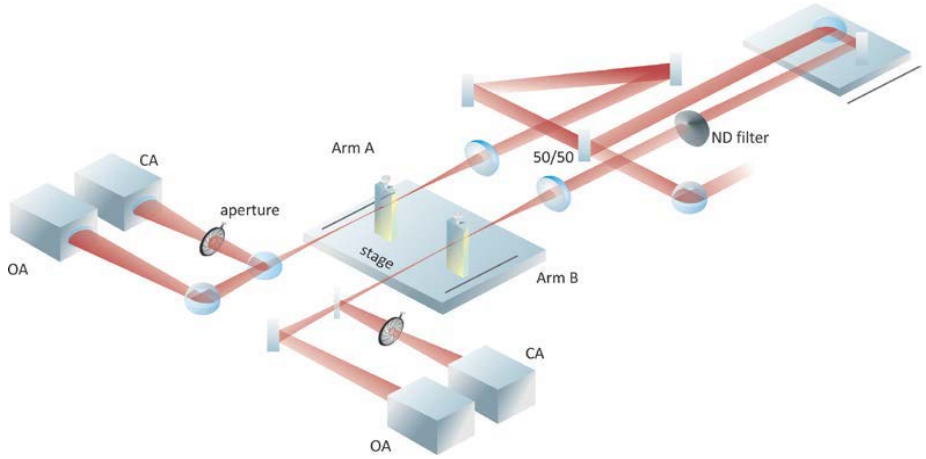

Figure 6. Schematic of dual-arm Z-scan. The items labeled CA and OA represent the closed aperture and open aperture detectors for each arm, respectively. The reference beam used for energy monitoring is not shown (from Ref. [28]).

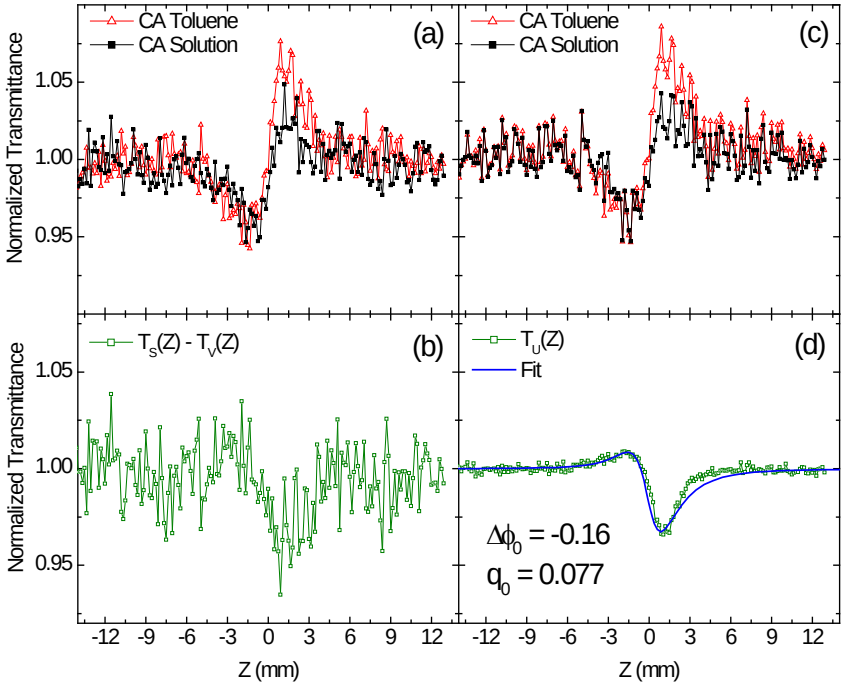

Figure 7. (a) Sequential CA single-arm Z-scans of the solvent toluene (open red triangles) and the solution of SD-O 2405 in toluene (closed black squares) at 695 nm where the concentration C = 47 μM, the pulse energy E = 31 nJ (I_0 = 51 GW/cm^2) and (b) the subtraction of the solvent CA signal from the solution CA signal (open green squares); Note this is for the same molecule as shown in Fig. 5. (c) Simultaneous CA dual-arm Z-scans of the solvent toluene (open red triangles) and the solution SD-O 2405 in toluene (closed black squares) at 695 nm using the same pulse and (d) the subtraction of the solvent CA signal from the solution CA signal after low-energy background signal (LEB(Z)) subtraction (open green squares) and corresponding fit of both 2PA and NLR (solid blue line) with $\Delta\phi_0$ = -0.16, q_0 = 0.077, using S = 0.33.[28]

3.1.3 Determining nonlinear response from pulsewidth dependence of Z-scans

Z-scans of materials exhibiting one-photon absorption (1PA) induced ESA (see Eqs. 9-12) cannot easily be distinguished from Z-scans performed on materials with only ultrafast nonlinearities. One way to distinguish is to perform the Z-scan at two different pulsewidths. If the Z-scans are identical for the same irradiance but different pulsewidths, the response time of the nonlinearity is shorter than the temporal width of the pulses used. For very short pulses, (e.g. femtosecond) this would indicate that the mechanism is 2PA. If the open aperture Z-scans are identical for the same fluence, then they may be due to ESA. Similarly, if the closed aperture Z-scans are the same for the same fluence rather than irradiance, then the nonlinear refraction may be due to the redistribution of the populations.

In order to illustrate this, we show Z-scan data for a sample of chloro-aluminum phthalocyanine (CAP) in Fig. 8 using a fixed energy, but pulswidths differing by a factor of two.[15] Thus the irradiance changes by a factor of two while the signals for both nonlinear absorption and nonlinear refraction are nearly identical. Both nonlinear absorption and refraction are due to excited states, rather than to 2PA and bound-electronic n_2.

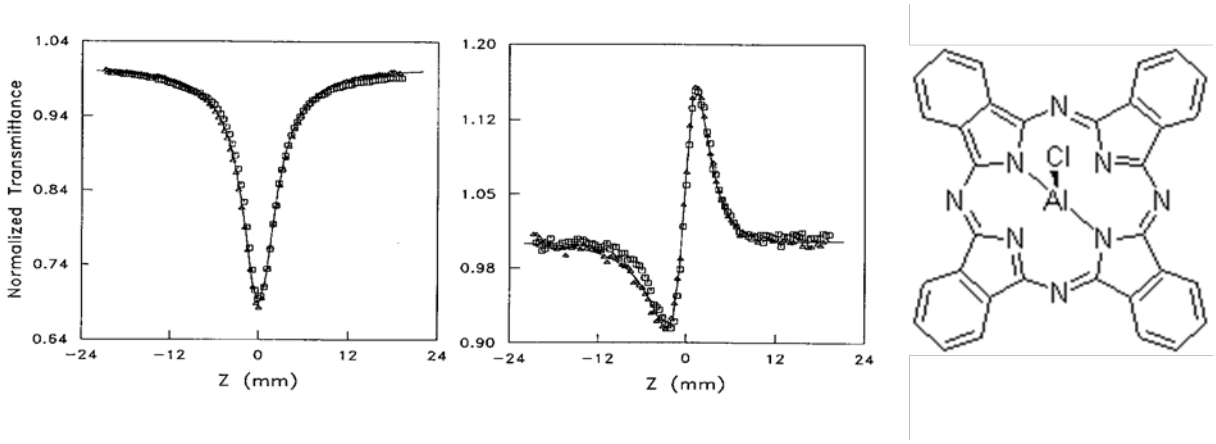

Figure 8. Open aperture Z-scan data at 532 nm using (open triangles) 30 ps pulses (FWHM), and (open squares) 62 ps pulses (FWHM) on Chloro-Aluminum Phthalocyanine – left, and closed aperture Z-scan data (divided by open aperture data) for the same pulsewidths – right. The molecule is shown at the right. From Ref. [15].

Creating new linear absorption resonances by creating excited states changes the index, and the sign depends upon which side of the resonance the light is - and additionally removing absorbers from the ground state also changes the index - again the sign depends on the resonance frequency and these contributions add to determine the net NLR. These can be determined by the usual Kramers-Kronig relations for the materials with the changed absorption profile, i.e. including the new ESA or saturated absorption profile. It is important to note that this is not an n_2 since it will depend on the density of excited states created, which is energy dependent.

When the excited states are created by 2PA, as described in Eq. 14, the NLA can mimic fifth-order 3PA while the nonlinear refraction also appears as a fifth-order NLR signal.[18, 38] Figure 9 shows a molecule where ESA and excited-state refraction occur due to 2PA.

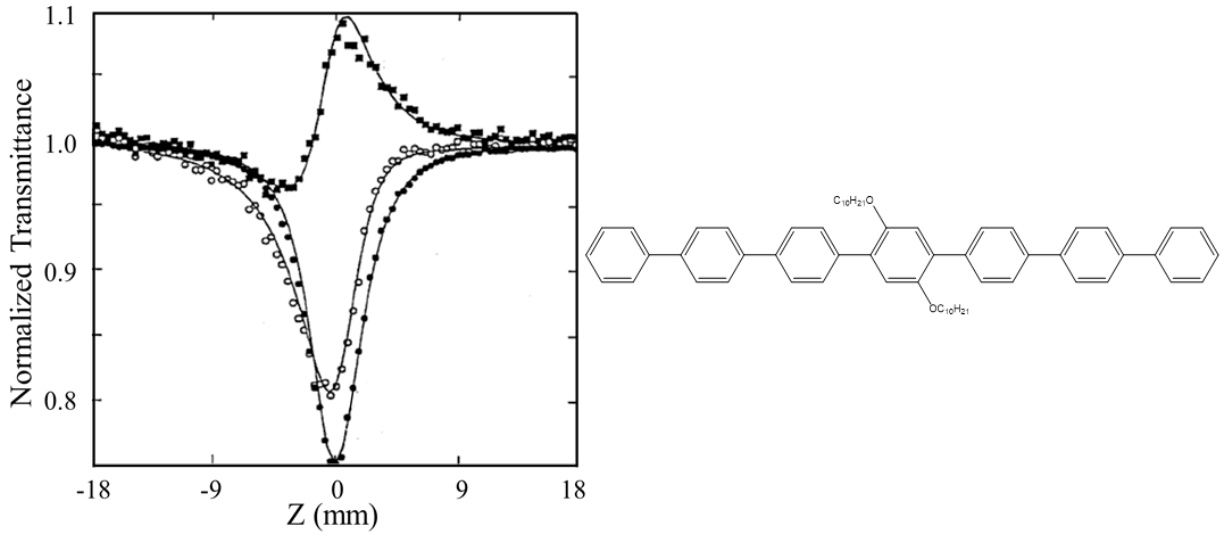

Figure 9. Open (open circles), closed (closed circles) and divided (closed squares) Z-scan data of the organic molecule shown on the right. The solid lines are fits to the data. From Ref. [38].

Here the equations are modified in a straightforward way following Eq. 14 but ignoring linear absorption. The irradiance varies as

$$\frac{dI(t)}{dz} = -\alpha_2 I^2(t) - \sigma_{ex} N_e(t) I(t) \tag{29}$$

while the excited-state generation varies as

$$\frac{dN_e}{dt} = \frac{\alpha_2 I^2(t)}{2\hbar\omega}. \tag{30}$$

While these don't have a simple solution as in the 1PA generated excited-state case, they can be numerically evaluated for Z-scans as shown in the fits of Fig. 9. Again, for a fixed irradiance longer pulses contain more energy, and the role of the ESA and ESR is increased. Some researchers have quoted effective 3PA coefficients for the NLA portion of these equations by temporally integrating the excited-state density. For example, assuming Gaussian temporal pulses of HW1/eM t_0 yields;

$$N_e(t) = \frac{\alpha_2}{2\hbar\omega}\int_{-\infty}^{t} I^2(t')dt' = \frac{\alpha_2 I_0^2}{2\hbar\omega}\int_{-\infty}^{t} e^{-2(t'/t_0)^2} dt' \tag{31}$$

which can be used in Eq. 29. If the pulses are long enough, the second term in Eq. 29 dominates, and since $N_e(t) \propto I^2$, the open aperture Z-scan signal looks like 3PA with $N_e(\infty) = \sqrt{\frac{\pi}{2}} \frac{\alpha_2 I_0^2 t_0}{2\hbar\omega}$, which when used in Eq. 29 yields an I^3 dependence for the spatial derivative of the irradiance. This provides a quick estimate of the size of the nonlinear absorption. However it also points out how easily this cascaded 2PA+ESA (i.e. $\mathrm{Im}\chi^{(3)}$):$\mathrm{Im}\chi^{(1)}$ effect can be misinterpreted in an experiment as 3PA.[18] The nonlinear refraction from creating these excited states also looks like a fifth-order "n_4" using similar math ($\mathrm{Im}\chi^{(3)}$:$\mathrm{Re}\chi^{(1)}$); however, again this doesn't give the essential physics behind the NLR.

3.1.4 White-Light-Continuum Z-scan (WLC Z-scan):

Performing nonlinear spectroscopy using Z-scan can be time consuming since most broadly tunable sources, e.g. optical parametric sources, require lengthy characterization each time they are tuned since the temporal, and in particular, the spatial profiles are not reproducible. Usually spatial filtering is required if Gaussian profile pulses are to be used. Again this is not a necessary condition for performing Z-scans but it greatly simplifies analysis.[39-41]

Nonlinear spectroscopy using Z-scan is possible as shown in Figure 10, where the 2PA spectrum of a squaraine molecule shown in the figure was measured by performing open-aperture Z-scans at many wavelengths using an optical parametric amplifier (OPA). Such a spectrum can take several days to perform, since the Z-scan needs to be realigned for each wavelength, as the OPA beam alignment changes upon tuning.[42]

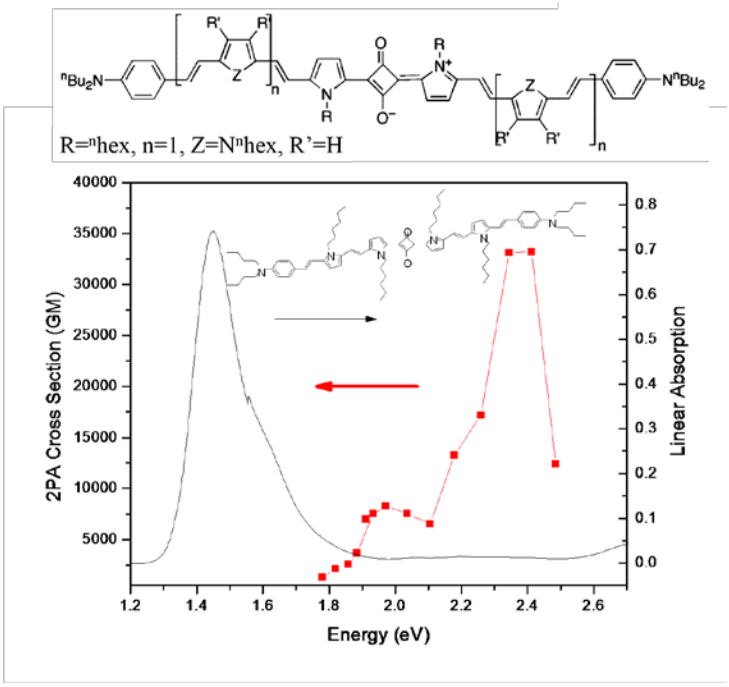

Figure 10. Linear absorption (right arbitrary axis) along with 2PA cross section (left axis) determined by open aperture Z-scans versus photon energy for the molecule shown. The energy corresponds to the energy of final excitation for both linear and two-photon absorption, e.g. the 2PA peak is near an input photon energy of 2.35/2 eV.[42]

A solution that allows rapid Z-scan characterization of materials over a broad spectral range is the white-light-continuum, WLC, Z-scan.[39-41, 43] Here the Z-scan methodology is the same but we replace the usual 'single' frequency source in the Z-scan with a spectrally filtered WLC.[44]

The apparatus is shown in Fig. 11. The WLC is produced by weak focusing in a long ~1.5 M cell filled with Kr gas at a pressure of ~2 atm. Using Gaussian spatial profile, femtosecond excitation pulses of ~1mJ at ~800nm produces a clean spatial profile pulse of spectral content from <400nm to >800nm, i.e. greater than 1 octave.

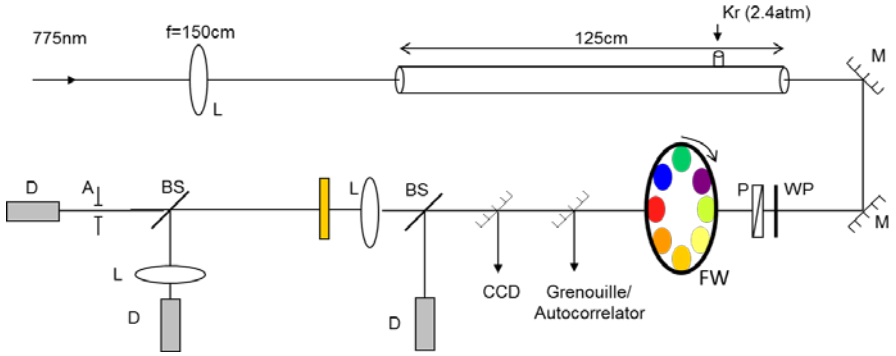

Figure 11. WLC Z-scan experimental setup: L: lens; M: mirror; WP: half-wave-plate; P: polarizer; FW: filter wheel; BS: beam splitter; D: detector; A: aperture; S: sample; the dotted M's are removable mirrors for beam characterization. From Ref. [40]

The entire WLC cannot be used in a single Z-scan since besides the degenerate 2PA there will be strong nondegenerate 2PA and these two processes cannot be simply separated. The simplest method to apply is to spectrally filter the WLC prior to the sample and perform a normal single frequency Z-scan. Then the spectral filter can be changed (e.g. using a computer controlled rotating platform holding many spectral filters as shown in Fig. 11, or using a linear variable filter) and another Z-scan performed.

The filters must be spectrally broad enough to support the pulses used, in our case ~ 100 fs. The difference between using the WLC and, for example, tuning an optical parametric generator/amplifier, OPG/A is in the length of time it takes to measure a nonlinear spectrum (or nonlinear dispersion curve). As it turns out, once characterized in terms of spatial properties at all wavelengths and temporal profiles at all wavelengths, the WLC is stable from day to day and week to week. This cannot be said of optical parametric sources. We have found that OPG/A's when tuned change their spatial profile and usually spatial filtering is needed to obtain Gaussian profile beams. Figure 12 shows the characterization of a WLC demonstrating that near Gaussian profile beams are obtaining at all the wavelengths over an octave span. New research is extending the useful range to > two octaves using different excitation wavelengths. Thus, once characterized, the WLC can be used to perform nonlinear spectroscopy while the OPG/A needs to be re-characterized after each tuning cycle.

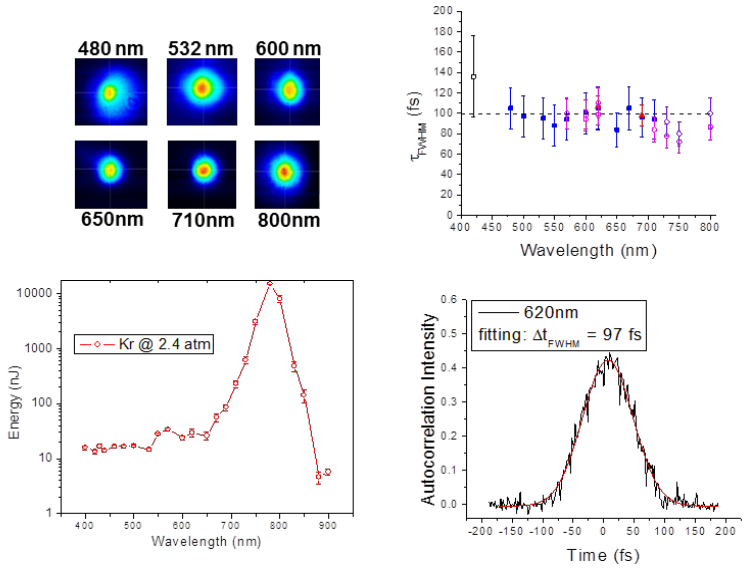

Figure 12. Characterization of the WLC. Spatial profiles - upper left, temporal pulsewidth - upper right, available energy after narrow band filters - lower left, example of an autocorrelation after a 620nm narrow band filter (~10 nm bandwidth) - lower right.[40]

This WLC Z-scan has the potential of serving as the nonlinear equivalent of a linear spectrophotometer. When automated, a researcher can insert a sample, initiate a measurement and then after some time (perhaps < 1 hour for kHz sources) retrieve the degenerate nonlinear absorption spectrum; however, with this nonlinear spectrophotometer there is the added benefit

not given by a linear spectrometer. The dispersion of the nonlinear refraction is measured simultaneously with the closed-aperture Z-scan as shown in Fig. 11. Using this configuration the data of Fig. 13 were taken.

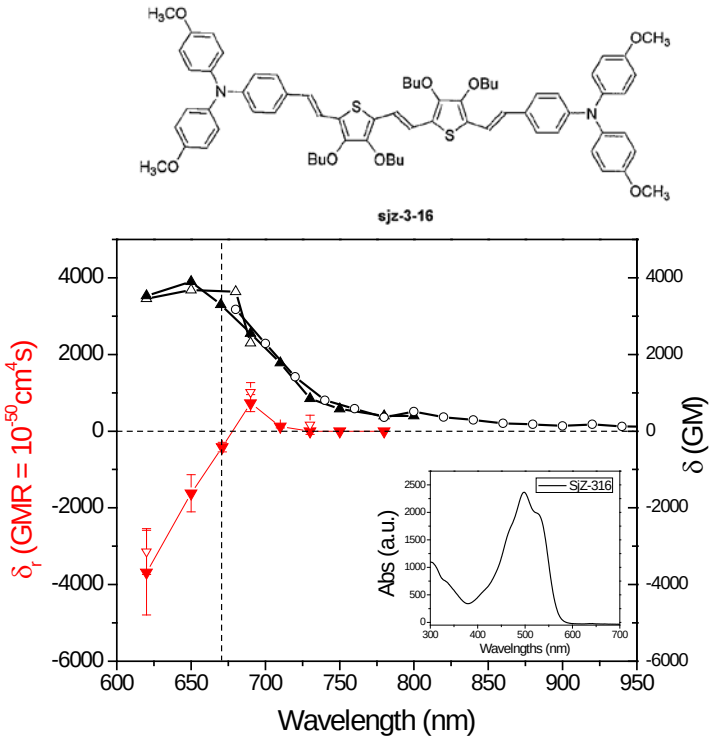

Figure 13. 2PA cross section, right axis, and nonlinear refractive cross section, left axis for the molecule shown to the right. Data taken using the WLC Z-scan, except for wavelengths longer then 800nm where 2-photon fluorescence is used (open circles). From Ref. [40]

3.1.5 Other Variants of the Z-scan method:

Determining the physical mechanism or mechanisms responsible for the signal is seldom revealed by a single Z-scan experiment although using ultrashort femtosecond pulses can sometimes limit the significant responses to bound-electronic nonlinearities.[45, 46] See Fig. 8 where either one of the Z-scans could have been used to extract erroneous values for a 2PA coefficient and an n_2. There have been many variations of the Z-scan introduced over the past years. Many of these have shown the potential to further increase the sensitivity, e.g. EZ-scan [29], while others have introduced multiple beams which have the potential to allow for measuring nondegenerate nonlinearities [27, 35, 47]. However, all these "improvements" come at the cost of complicating the methodology, and the simplicity of this technique is the likely reason it became so popular.

The 4f coherent imaging method [48] and many other techniques are closely related to Z-scan. Here, for example, a beam profile is focused through a nonlinear sample and imaged in the linear regime. Then the irradiance is increased and the change in the imaged irradiance distribution is observed. The nonlinearly induced phase distortion can be calculated and the nonlinear index

determined. Nonlinear absorption can also be analyzed. In the particular reference given [48], a circular flat-top beam is imaged and the light going into the originally dark area in the image plane is monitored. When fully aligned the nonlinear index (and/or absorption) can be determined in a single shot.

As previously stated, the Z-scan technique is sensitive to ALL NLA processes and ALL NLR mechanisms. Unraveling the various physical processes that contribute to these nonlinearities cannot be unambiguously determined with single Z-scans.

3.2 Indirect Methods

By indirect we mean that a material is excited optically to be sensed by some other means than the transmission of the excitation beam itself. These other means could include measuring the transmittance of a probe, heating of materials, fluorescence, etc. For example, an excitation beam induces excited states via 2PA whose presence are sensed by their fluorescence whose intensity is proportional to how many excited states were produced via 2PA. We give examples of these indirect methods in the following.

3.2.1 Excitation-Probe Methods:

Figure 14 shows the standard excite-probe experimental setup where an excitation pulse is incident on the system at time $\tau_d = 0$ and the probe pulse examines the change in transmission properties of the sample at later times $\tau_d > 0$. For example, see articles in Ref. [49]. The excitation and probe pulses could be at the same (degenerate) or different (nondegenerate) wavelengths but in order that they are synchronized in time they must be derived from the same pulsed laser source. The time delay, τ_d, of the probe is controlled by a delay line as shown in Fig 14.

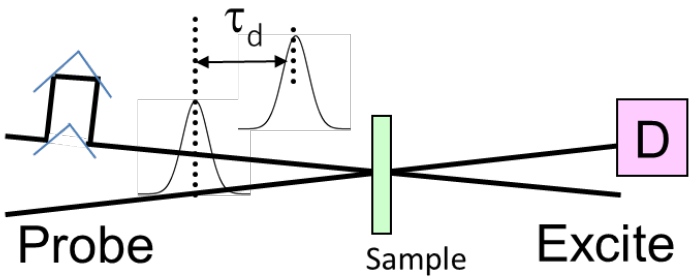

Figure 14. Excite-probe experimental setup showing the optical delay line.

Two-photon absorption can easily be differentiated from ESA using excite-probe techniques since for times after short pulse excitation (pulsewidth shorter than the decay time of the system τ), the ESA will be present after the excitation pulse is over, i.e. for τ greater than the pulsewidth. For example, for 1PA generated excited states the dynamics are described by a modification of Eq. 9 that includes simple decay

$$\frac{dN_e}{dt} = \frac{\sigma_{ge} N_g I_e}{\hbar\omega} - \frac{N_e}{\tau} \quad , \tag{32}$$

where definitions are as given in Sec. 2.1, I_e is the excitation irradiance and τ is the decay time. It is assumed that the probe irradiance is weak enough that it generates no significant excited-state population. The transmission change is sensed as a function of time delay by the probe pulse, according to

$$\frac{dI_p}{dz} = -(\sigma_{ge}N_g + \sigma_{eu}N_e)I_p. \tag{33}$$

Provided the excitation and probe pulses are much shorter than the decay time, τ, integration over time to find the probe fluence is straightforward. Defining the probe fluence transmittance as, $T_{probe}(\tau_d) = F(\tau_d, L)/F(\tau_d, 0)$, and the normalized transmittance as $T_{NL}(\tau_d) = T_{probe}(\tau_d)/T_L$, where T_L is the linear transmittance of the probe, we find,

$$T_{NL}(\tau) = [T_{NL}(0)]^{(\exp(-\tau_d/\tau))} \tag{34}$$

where $T_{NL}(0) = \left[1 + \frac{(\sigma_{eu}-\sigma_{ge})F_e}{2\hbar\omega}\left(1 - e^{-\alpha_0 L}\right)\right]^2$ is the probe fluence transmission for the probe delay immediately after the excitation pulse. Here we have assumed that $\alpha_0 = \sigma_{ge}N_g$ is constant, i.e., small depletion of the ground state. Provided the changes in normalized transmittance are small, i.e. $\Delta T = 1 - T_{NL} \ll 1$ then Eq. 34 becomes

$$\Delta T_{NL}(\tau) \cong \Delta T_{NL}(0)e^{-\tau_d/\tau}, \tag{35}$$

so that the transmittance change can be simply fit with an exponential decay to determine the excited-state lifetime. Meantime the excited-state absorption cross section, σ_{eu}, can be determined from $T_{NL}(0)$. Even if we do not satisfy the conditions for Eq. 35, we may still fit the decay with Eq. 34; however, provided we remain in this low-excitation regime where there is small depletion of the ground state population, we do not need to know the molecular density to obtain σ_{eu}. Figure 15 shows an example of an excite-probe experiment on a squaraine molecule (SD 2577) at a wavelength of 532 nm with 30 ps pulses.[50]

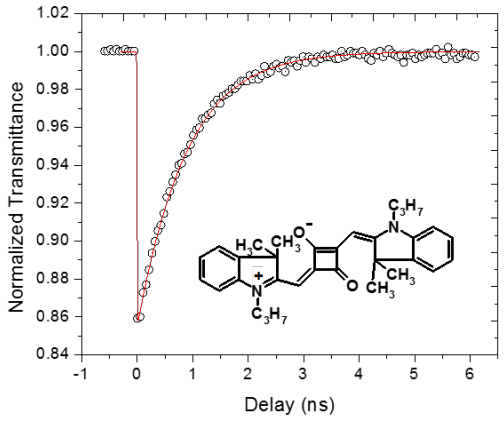

Figure 15. Excite-probe on the squaraine molecule shown in the inset (SD 2577) at a wavelength of 532 nm, showing ESA with a decay time of 0.9 ns. Details are given in Ref. [51].

This single excite-probe experiment can often determine the singlet manifold molecular parameters, but it is usually incapable of determining the triplet yield, cross section, and lifetime which are often important for organic dyes. This can be done using a double excite-probe geometry as discussed in detail in Ref. [52]. In these experiments a first excitation creates a population of the triplet state which is excited again after allowing sufficient time to create a triplet population and then probed to determine these molecular constants.

While degenerate excite-probe methods are probably best for fully understanding the mechanisms involved in a single-beam experiment such as Z-scan, it is often useful to perform nondegenerate excite-probe measurements, where the excitation and probe are at different wavelengths. Experimentally, this has the advantage that the weak probe can be easily distinguished from the strong excitation beam using spectral filters, but using different excitation and probe wavelengths allows other measurements to be performed. This allows, for example, the entire excited-state absorption spectrum to be measured by tuning the probe while keeping the excitation wavelength fixed.[53] Also the excitation beam can be used to generate excited states via two-photon absorption which has the advantage of creating a more uniform excitation through the depth of the sample. Finally, there may be nondegenerate 2PA involving the absorption of one photon from each of the excitation and probe beams. In this case, the propagation equations for the probe and excitation beams are,

$$\frac{dI_p}{dz} = -2\alpha_2(\omega_p;\omega_e)I_eI_p - \sigma_{ex}(\omega_p)N_eI_p \qquad (36)$$

$$\frac{dI_e}{dz} = -\alpha_2(\omega_e;\omega_e)I_e^2$$

where $\alpha_2(\omega_p;\omega_e)$ is the nondegenerate 2PA coefficient, and it is assumed that there is no ESA experienced by the excitation beam. In the event that there is degenerate 2PA at the excitation wavelength, the excited-state population is given by,

$$\frac{dN_e}{dt} = \frac{\alpha_2(\omega_e;\omega_e)I_e^2}{2\hbar\omega} \qquad . \qquad (37)$$

As illustrated in Fig. 1 (right), the effects of these excited states may be seen by the presence of ESA after the excitation pulse, and since the excited-state density is proportional to I_e^2, the ESA experienced by the probe will appear as a higher-order nonlinearity than the nondegenerate 2PA, which is proportional to I_e. With femtosecond pulses, the population densities generated by 2PA are usually too small for significant ESA to be observed. However, Fig. 16 shows a lead bis(ethynyl)porphyrin polymer where 2PA-generated ESA is large using femtosecond excitation.[54] Figure 16 shows excite-probe data for two excitation energies differing by a factor of 2 along with fits using 2PA excitation of state e followed by ESA to state u. In this case, there is actually a multilevel excited-state system where the 2PA-excited state decays to a lower-lying state in ~240 fs which leads to the delay of the onset of ESA. The ESA scales as the input energy squared while at zero delay there are contributions from both 2PA, which scales linearly with the energy, and ESA.

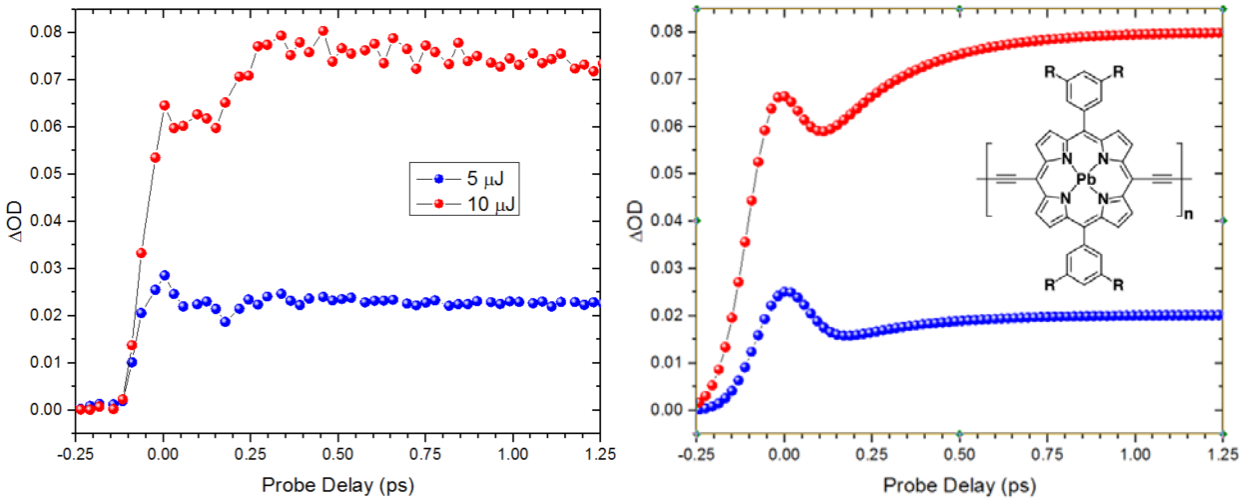

Figure 16. Left - excite-probe data showing the change in optical density on the lead bis(ethynyl)porphyrin molecule shown in the inset right, versus temporal delay for excitation energies differing by a factor of 2. Right – fits for the two energies on the left using a combination of 2PA and ESA. Data and fits provided by Joel Hales from Ref. [54].

3.2.2 White-Light Continuum (WLC) Excite-Probe Spectroscopy:

Excitation-probe experiments using a WLC probe as shown in Fig. 17 have greatly speeded data acquisition of nondegenerate nonlinear absorption spectra since tuning of the probe becomes unnecessary.[55-57] A commercial product based on WLC Excite-Probe Spectroscopy has been developed by Helios Inc.

Usually a femtosecond excitation pulse is used, which is also used to create a femtosecond WLC. Here, the probe (WLC) irradiance is kept weak to avoid any nonlinear effects induced by the probe itself. Then, in most cases the entire WLC can be incident on the sample at the same time; however, care still needs to be applied since linear absorption of the WLC can produce excited states. Thus the femtosecond excitation prepares the sample to be probed by the WLC which can be temporally delayed to give the spectral dynamics of the NLA. A WLC reference can also be used to give the linear transmittance spectrum which can be used to determine the nonlinear change in transmittance at all WLC wavelengths as a function of temporal delay.[57]

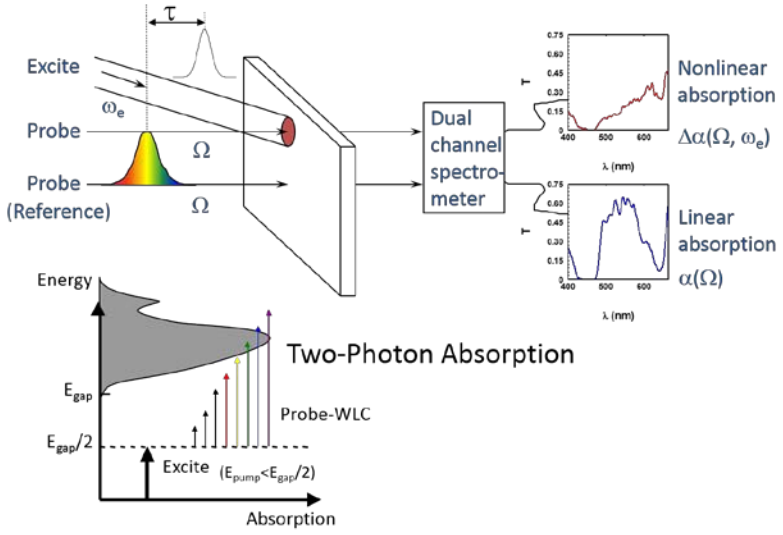

Figure 17. Femtosecond excitation, white-light continuum probe spectroscopy setup showing a 2PA measurement.[57]

The WLC probe may be used to measure the nondegenerate 2PA spectrum, $\alpha_2(\omega_p;\omega_e)$ as described by Eq. 36. Figure 18 shows a nondegenerate nonlinear absorption spectrum of the molecule shown for different excitation wavelengths giving different levels of nondegeneracy. For the largest nondegeneracy the nonlinear response is enhanced the most due to intermediate-state-resonance enhancement (ISRE), i.e., 2PA becomes larger if the intermediate state becomes closer to being one-photon absorbed.

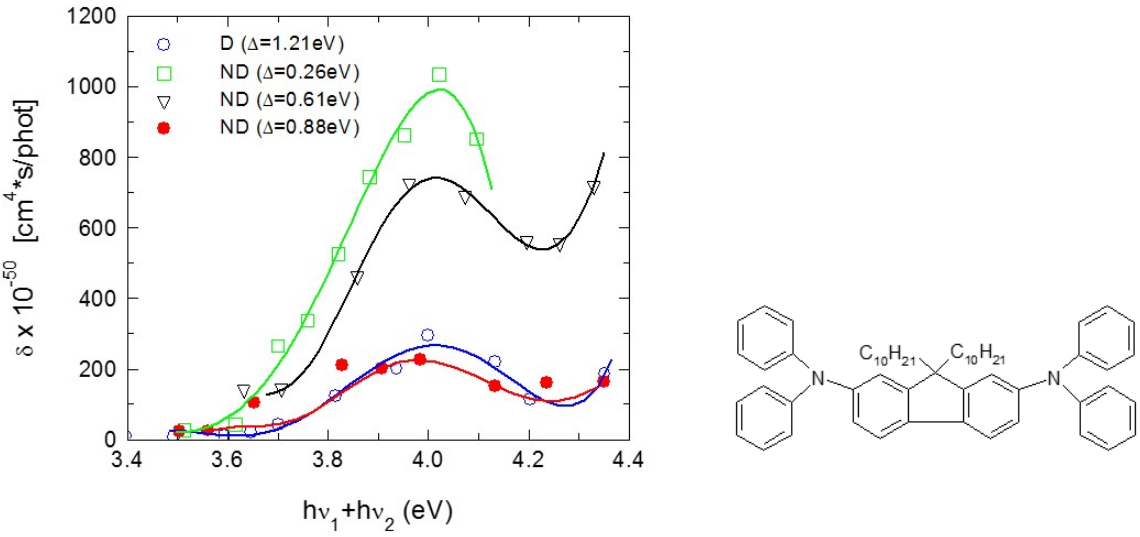

Fig. 18. Two-photon absorption spectrum of the molecule on the right as a function of the photon energy sum for different excitation photon energies from degenerate, D (blue circles) to very nondegenerate, ND (green squares).

Additionally, by tuning the excitation wavelength to a linear absorption band and delaying the WLC probe by a few ps with respect to the excitation pulse, we can measure the induced absorption of the probe over a broad wavelength range to obtain the ESA spectrum. Figure 19 shows the ground state and ESA spectrum of a thiacarbocyanine dye which was obtained with a 120 fs (FWHM) excitation pulse at 900 nm and a 117 fs (FWHM) white-light probe pulse, delayed by 13 ps with respect to the excitation pulse over the spectral range of 400–800 nm. In this case, we observe an excited-state cross-section that is ~3 times larger than that of the ground state cross section at the peak spectral position, while the integrated areas of their absorption bands are nearly the same.

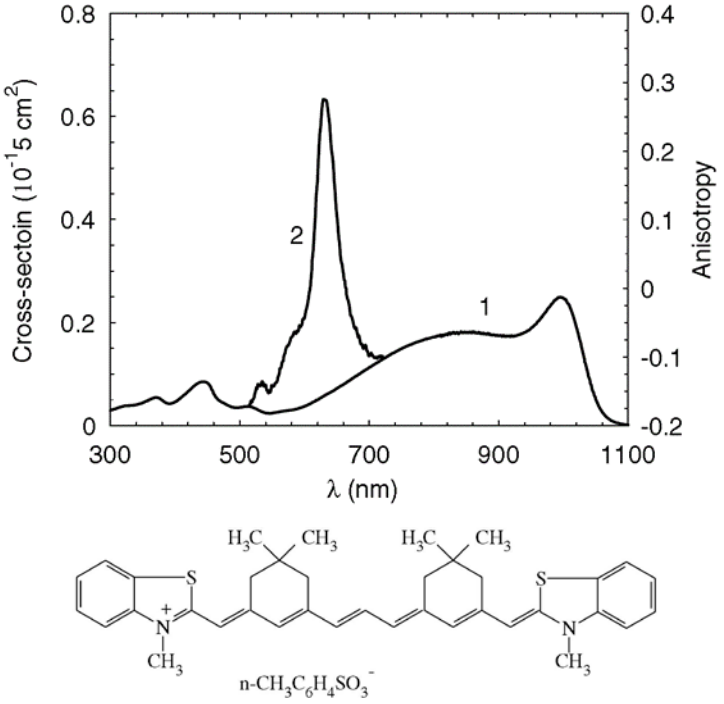

Fig. 19. Ground-state absorption (1) and ESA spectrum (2) for the molecule shown at the bottom. [58]

Unfortunately there are other experimental artifact signals that appear in this technique that require subtraction to obtain the signals of interest. References [55, 56] describes how to do this. The resultant excite-probe data can be fit using a single equation that depends on the WLC chirp, the group-velocity dispersion (GVD), the excitation irradiance, and the sample's nondegenerate nonlinear absorption. The GVD and the WLC chirp can be measured using the same apparatus of Fig. 17 by adding appropriate polarizers as in the optical Kerr effect measurement.[59] This excite-probe spectroscopic method is useful for measuring both 2PA and ESA and can distinguish between these nonlinearities since two-beam experiments show the temporal dynamics.

If the nondegenerate nonlinear absorption spectrum obtained is broad enough to cover all the spectral features, Kramers-Kronig relations can be applied to calculate the nondegenerate nonlinear refraction dispersion.[9, 60, 61] In addition to the WLC probe for measuring NLA, a narrower spectrum ultrashort probe pulse can be spectrally resolved to give remarkably sensitive measurements of NLR in addition to giving the NLA. Here, the reported sensitivity to a nonlinearly-induced phase change is ~10^{-7} waves.[62, 63] This method was first used by

Mysyrowicz to measure the nonlinear refraction of air and temporally resolve the various nuclear components coming from N_2, and O_2. By spectrally resolving the transmitted probe pulse, the cross-phase modulation, XPM, can be seen as a time-dependent shift of the frequency.[63]

3.2.3 Degenerate Four-Wave Mixing, DFWM

Another excite-probe measurement is degenerate four-wave mixing, DFWM, but in this case uses two excitation beams. For short-pulse nonlinear measurements a standard geometry is shown in Fig. 20 where all beams can be temporally delayed. The excitation beams are usually the forward and backward excitation beams which are counter-propagating, while the probe comes in at a small angle with respect to the forward excitation. The analysis usually involves discussions of the multiple gratings produced which scatter the various beams in the phase-conjugate or signal direction which is backward propagating from the probe. In addition to the usual grating terms there is a so-called two-photon coherence term which also results in signal.[64-66] The PC signal using this geometry in the low depletion (small signal) limit is:

$$\left|\chi_{eff}^{(3)}\right|^2 \cong \frac{n_0^4 c^4 \varepsilon_0^2}{\omega^2 L^2} \frac{I_c}{I_f I_b I_p} \quad , \tag{38}$$

and the spot sizes and pulsewidths of the PC signal are: $w_{PC}^{-2} = w_f^{-2} + w_b^{-2} + w_p^{-2}$ and $\tau_{PC}^{-2} = \tau_f^{-2} + \tau_b^{-2} + \tau_p^{-2}$ respectively. The important result to note is that the nonlinear susceptibility phase is not given; thus both real and imaginary parts contribute to the PC signal and they cannot be separated without determining this phase. Various homodyne and heterodyne techniques have been developed but often add a great deal of complication.[67, 68] The geometry discussed next can simplify this problem.

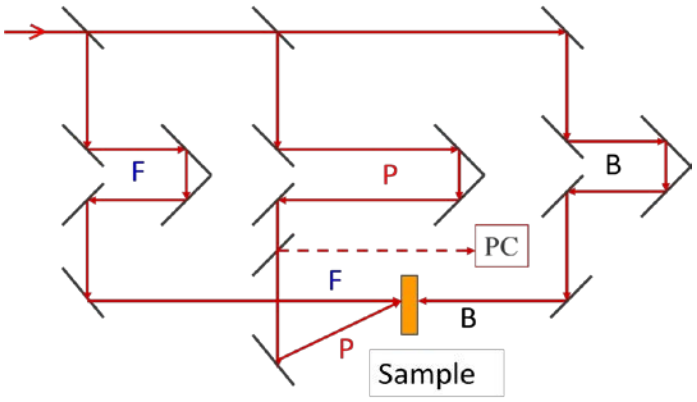

Figure 20. DFWM setup for pulsed measurements. F,B and P refer to the forward excitation, backward excitation and probe beams respectively. PC is the phase conjugate beam or signal which is detected.

Another standard geometry is the so-called boxcar geometry shown in Fig. 21 where three input beams (four where homodyne detection is used to determine the phase) are arranged to give a PC/signal beam which forms the fourth corner of the "box".[69] If the phase of the signal with respect to the excitations can be measured, this allows separation of the absorptive and refractive nonlinearities. These beams can be generated using diffraction gratings (2D gratings can produce all the needed beams from a single input and essentially eliminate the need for phase stabilized beams).[69, 70]

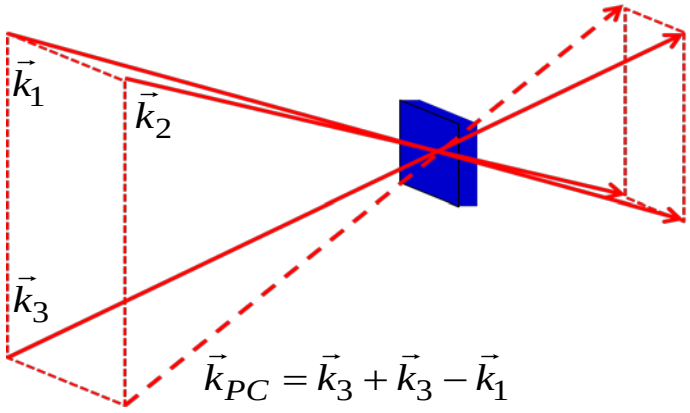

Figure 21. Boxcar geometry for DFWM. The dashed line is the phase matched signal/PC. For homodyne detection a weak beam is also incident along this direction to obtain phase information.

The magnitude of the nonlinear susceptibility can be determined with the use of a known reference sample from;

$$\left|\chi_s^{(3)}\right| = \left|\chi_r^{(3)}\right| \sqrt{\frac{I_s}{I_r}} \left(\frac{n_s}{n_r}\right)^2 \frac{L_s}{L_r} \left[\frac{\ln T}{\sqrt{T}\left[1-T\right]}\right] \tag{39}$$

where L is the sample length, subscripts s and r refer to the sample and reference respectively, and T is the linear transmittance of the samples. Here the reference sample is assumed to be nonabsorbing and the experimental conditions identical. The signals from the reference and sample are I_r and I_s which are the maxima in the DFMW signals with time delay. Figure 22 shows an example of a DFWM signal in the boxcar geometry without homodyne detection on a sample of carbon disulfide, CS_2, where the solid line comes from a calculation of the expected signal from the known response function determined in Ref. [70].

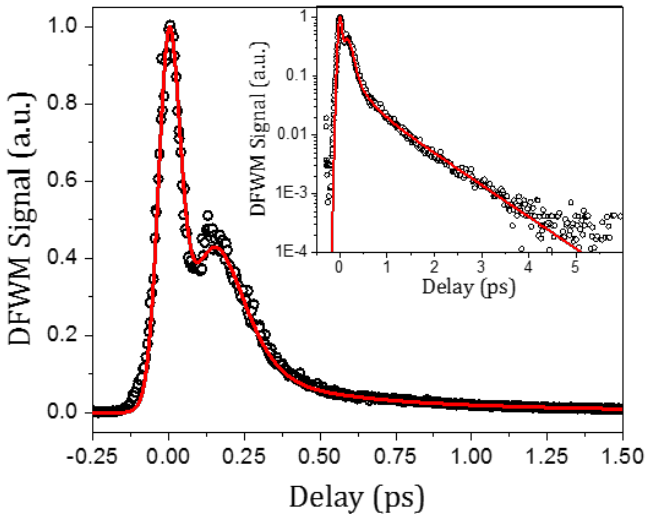

Fig. 22 DFWM data as a function of the probe time delay using the boxcars geometry on CS_2 for 88 fs and 42 fs pulse widths of the excitation and probe pulses, respectively at 700nm. The solid line is a fit using the bound electronic and nuclear responses as discussed in Ref. [70] Inset using a logarithmic vertical axis. Taken from Ref. [70]

3.2.4 Two-Photon Absorption Induced Fluorescence Spectroscopy

Many organic molecules show significant fluorescence quantum yields. This allows measurements of both one photon and two-photon absorption induced fluorescence (2PF) to obtain a degenerate 2PA spectrum. A typical experimental setup is shown in Fig. 23.

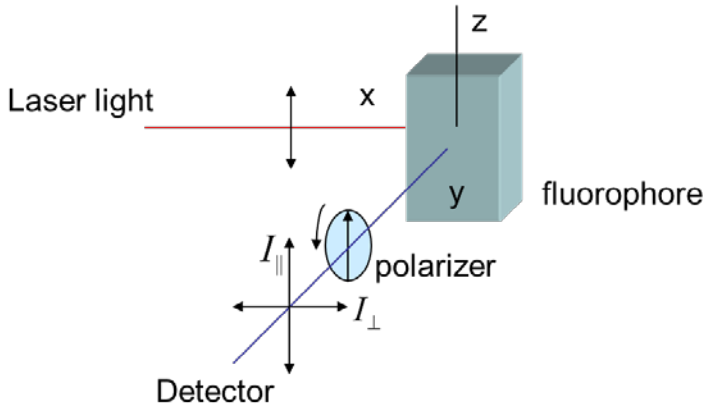

Figure 23. Experiment schematic for the two-photon fluorescence measurements

After simultaneous absorption of two photons, the excited state, rapidly relaxes to the zero vibrational level of the 1st excited state). The fluorescence intensity is a measure of the population of the first excited state, which is proportional to the 2PA coefficient. Since the 2PA is proportional to the square of the input irradiance, *I*, the resulting fluorescence signal is also

proportional to I^2. This dependence is thus a standard criterion to distinguish 1PF from 2PF which was first used by Kaiser and Garrett in 1961,[71] just one month after second harmonic generation was reported.[72] This technology was further developed to measure 2PA spectra [73, 74], and for two-photon microscopy.[75, 76] Due to the uncertainty of various experimental parameters, e.g., collection geometry and efficiency, absolute calibration of the fluorescence signal to determine the 2PA is problematic. Standard reference molecules with known 2PA spectra are often used to measure relative optical fluorescence signals.[73] When using 2PF to determine 2PA spectra as shown in Fig. 23 one needs to minimize strong re-absorption of the fluorescence signal for high sample solution concentrations by focusing the excitation beam near the wall of the cuvette close to the collecting lens. The fluorescence spectrum also needs to be corrected for the spectral sensitivity of the detector and for any residual re-absorption by the solution. To determine the 2PA spectrum of the sample solution, the integrated fluorescence signal is then compared to a reference molecule with known 2PA cross section under identical measuring conditions. The 2PA cross section for the sample can then be calculated from:

$$\delta_{2PA\,sample} = \frac{\langle F \rangle_{sample} n_{sample}^2 \Phi_{F\,ref} C_{M\,ref} \langle P \rangle_{ref}^2}{\langle F \rangle_{ref} n_{ref}^2 \Phi_{F\,sample} C_{M\,sample} \langle P \rangle_{sample}^2} \delta_{2PA\,ref} \tag{40}$$

where <F> is the integrated fluorescence and <P> is the average excitation power which is proportional to pulse energy, C_M is the concentration of the solution measured by measuring the 1PA spectrum and Φ_F is the fluorescence quantum yield measured by 1PF.

There are several other factors contributing to accurate 2PF measurements. The concentration of the solution should be as high as possible (but below the aggregation threshold) to increase the probability of 2PA, thus reabsorption can be a significant issue. Assuming the fluorescence spectrum and quantum yield are independent of the concentration of the solution and the type of excitation (i.e. 1PA or 2PA), the 2PF spectrum can be fit to the 1PF spectrum measured at lower concentration (with peak OD < 0.1) to obtain a correct spectral contour. The selection of a reference molecule is based on the spectral range of the fluorescence of the sample. A large overlap of the fluorescence spectra helps minimize the measurement error induced by the spectral sensitivity of the detector. Several 2PF standards have been published with emission wavelengths ranging from 390 to 1000 nm and excitation wavelength from 500 to 1600 nm.[73, 77, 78] However, there are still spectral ranges where new/more standards are needed.

Figure 24 shows the 2PF spectrum of an organic dye dissolved in chloroform calibrated against a known standard.[78] Z-scans of the 2PA spectrum are also shown and give agreement with the 2PF data.

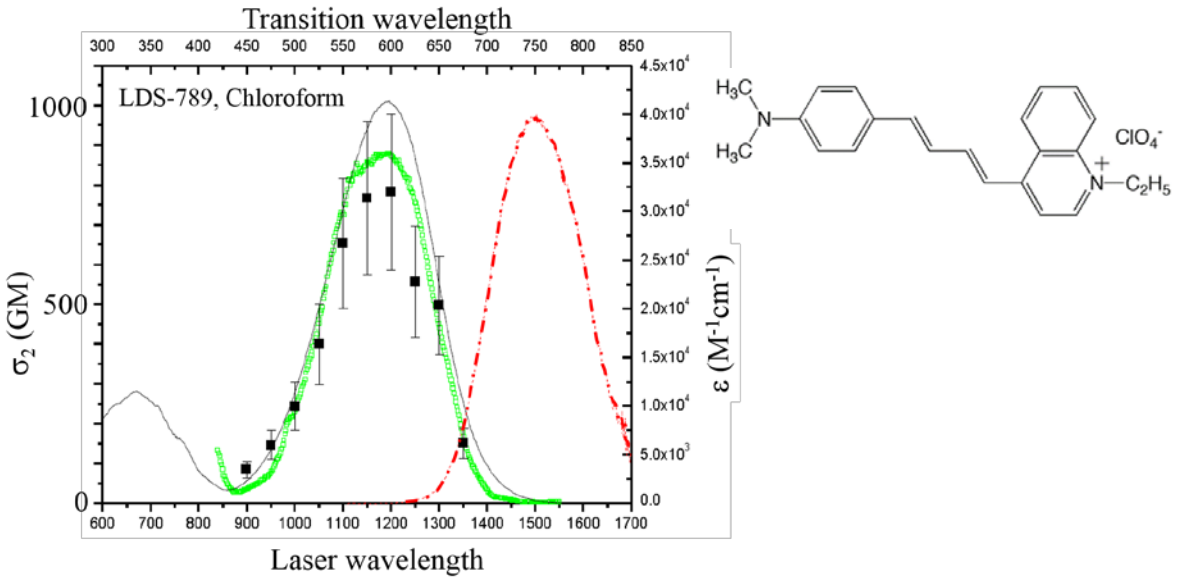

Figure 24. Linear absorption spectrum (black line, right vertical and top horizontal scales), normalized fluorescence spectrum (red dash-dot line, top horizontal scale), 2PA spectrum using reference calibrated 2PF (green symbols, left and bottom scales, and 2PA spectra by Z-scan (Black squares) of the molecule shown on the right. From Ref. [78].

2PF spectroscopy is in principle a rapid experimental technique to measure 2PA spectra in comparison to other commonly adopted techniques, e.g. Z-scan. However, verifying the quadratic dependence on irradiance at each wavelength considerably lengthens the experimental time. It is also not sensitive to the ESA that can follow 2PA, since the ESA doesn't contribute to the fluorescence. The sensitivity of 2PF can be very high, thanks to the high responsivity of PMT detectors and the fact that 2PF is a zero background signal technique. A 2PA cross section of ~ 1 GM can be measured given a sample solution with large fluorescence quantum yield at high concentration.

However, there are molecules whose fluorescent quantum yield is too low to measure by 2PF. It is also difficult to measure 2PA spectra of solid-state samples since reference material geometries will be difficult to match although the relative spectral shape of 2PA spectra can be determined Finally, the 2PF technique can only measure 2PA, i.e. imaginary part of $\chi^{(3)}$. The nonlinear refractive index, n_2, has to be measured by other experimental techniques.

3.2.5 Fluorescence Anisotropy

One-photon excitation fluorescence anisotropy measurements, especially when linked to quantum-chemical calculations, can reveal the spectral positions and orientations of the transition dipole moments from the ground state S_0 to the first excited state S_1 (μ_{01}) and to higher excited states S_n (μ_{0n}) relative to the orientation of the emission dipole moment (μ_{10}) . This information cannot be fully obtained from linear absorption spectra. The excitation anisotropy spectrum, $r(\lambda)$, is defined as,

$$r(\lambda) = \left[I_{||}(\lambda) - I_{\perp}(\lambda)\right] / \left[I_{||}(\lambda) + 2I_{\perp}(\lambda)\right], \tag{41}$$

where $I_{||}$ and $I_{\perp}$ are the fluorescence intensities polarized parallel and perpendicular to the excitation light respectively.[79] The angle, β, between the absorption transition moment and the emission transition moment can be determined from:[74]

$$r = \frac{2}{5}\left(\frac{cos^2\beta - 1}{2}\right). \tag{42}$$

Similarly, 2PA anisotropy can be measured by 2-photon excitation and measuring the ratio of parallel and perpendicular polarizations which for a 3-level system gives r_{2PA} as:[80]

$$r_{2PA} = \frac{18\cos(\gamma/2 - \beta_{01})\cos\beta_{01}\cos\gamma/2 - 7\cos^2\gamma/2 + 1}{7\left(2\cos^2\gamma/2 + 1\right)} \quad . \tag{43}$$

Here γ is the angle between dipole moments participating in the 2PA process, and β_{01} is the angle between the bisector of γ and the emission transition moment, which can be found from one-photon anisotropy measurements in Eq. 42.[81]

Shown in Fig. 25 is the fluorescence anisotropy spectra for both one and 2PA for a squaraine dye along with other data described in the next section.[82]

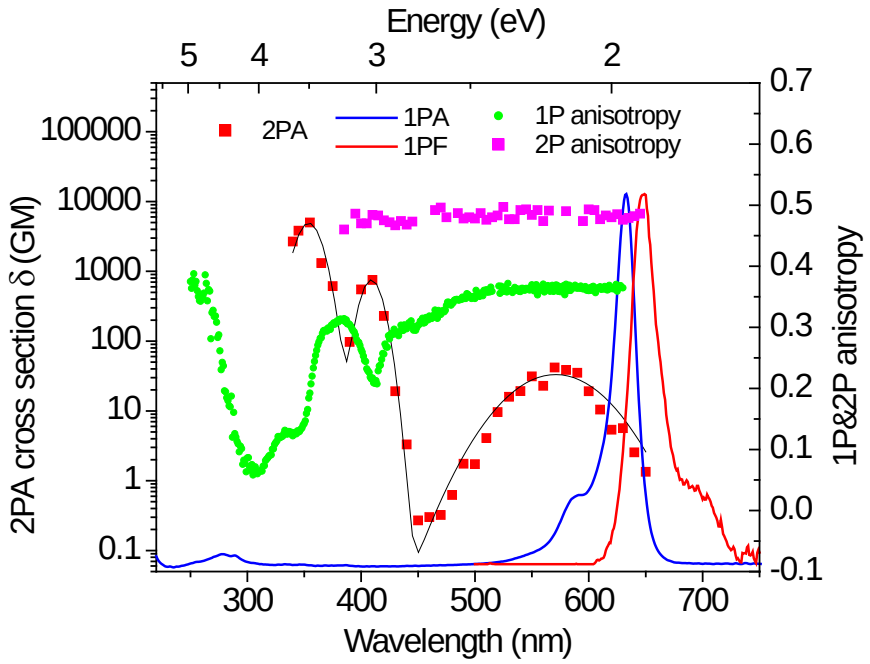

Figure 25. Shows the linear absorption spectrum (blue line) of the squaraine molecule (SD 2577 shown in Fig. 15) with the 1-photon fluorescence, 1PF (red line), 1PF anisotropy (green circles), 2PF anisotropy (purple squares), and the 2PF and Z-scan measurements (red squares) of the 2PA spectrum.[82] Black line is a model of the 2PA spectrum based on a single intermediate-state and three 2PA states, as described in Ref. [82].

4. EXAMPLES OF USE OF MULTIPLE TECHNIQUES

In this section, we describe how organic dyes are characterized by the combined use of several methods. Figure 24 already showed a dye where both 2PF and Z-scan were used to measure the 2PA spectrum, and Fig. 25 shows multiple data for a squaraine dye described below.

4. 1. Squarine Dye

Figure 25 shows the results of both linear and nonlinear spectroscopy of a Squaraine dye first reported in Ref. [82]. The linear absorption was measured in solution in ethanol using a spectrophotometer revealing a peak absorption wavelength at 632 nm with a peak extinction coefficient of $3.1 \times 10^{-5}\, M^{-1} cm^{-1}$. The fluorescence spectrum and fluorescence anisotropy were measured in dilute solution using a spectrofluorimeter from PTI, Inc. As described above, the one-photon excited fluorescence anisotropy reveals the position of the one and two-photon transitions, which usually cannot be determined from the linear absorption spectrum.[79] Also shown in Fig. 25 is the 2-photon excited anisotropy, which shows a constant value at all wavelengths measured. The 2PA spectrum shown is obtained by a combination of 2PF and Z-scan measurements, where the 2-photon fluorescence is measured at every wavelength and in each case the square-law dependence of fluorescence on excitation energy was verified while the Z-scan was measured at three wavelengths to provide an absolute calibration of the magnitude of the 2PA cross section.

The experimentally observed 2PA spectrum for SD 2577 includes 3 bands: a weakly allowed band at the vibronic shoulder of the $S_0 \rightarrow S_1$ transition, a more intense band at $\lambda = 408\, nm$ with $\delta_{2PA} = 760\, GM$, and a much more intense band at $\lambda = 350\, nm$ with $\delta_{2PA} = 5200\, GM$. The 2PA spectrum for this molecule can be directly mapped onto the anisotropy function $r(\lambda)$. The observed dips in anisotropy at 410 nm and at 345 nm correspond to the peak positions of the 2PA bands. The last dip at 309 nm corresponds to a position near twice the energy of the main $S_0 \rightarrow S_1$ absorption band. As a result, the 2PA cross section at this energy (corresponding excitation wavelength is 618 nm) cannot be experimentally determined due to linear absorption.

4.2 Tetraone Dye

The characterization of this dye, labeled TD2765 shown in Fig. 26, is similar to the squaraine dye described above. The methodologies are similar to those described in Sec. 4.1 and the results are shown below in Fig. 26.

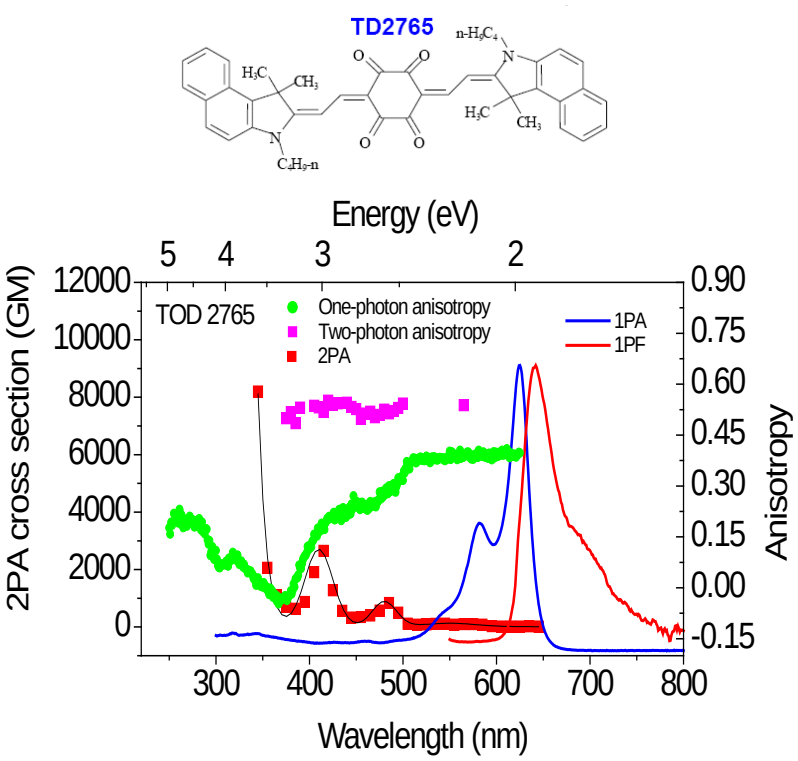

Figure 26. Linear absorption spectrum (blue line) of the tetraone molecule (TD2765) shown on the left along with the 1-photon fluorescence, 1PF (red line), 1PF anisotropy (green circles), 2PF anisotropy (purple squares), and the 2PF and Z-scan measurements (red squares) of the 2PA spectrum. Solid black line is a model of the 2PA spectrum based on a single intermediate-state and three 2PA states. Structure of TD2765 shown above plot. From Ref. [83].

The 2PA spectrum in this case was also taken using a combination of 2PF and Z-scan methods. However, close to the linear absorption edge, ($\lambda \approx 700\ nm$) the Z-scan gives 2PA cross sections as large as 35,000 GM. Since this is very close to the linear absorption region, one must be cognizant that ESA from excited states produced by 1PA can easily be mistaken for 2PA, as described in Sec. 2. The best means of determining the mechanisms for the nonlinear absorption in such cases is to perform excite-probe measurements, since the 2PA has an ultrafast response while the ESA will have a decay time equal to the fluorescence lifetime, typically hundreds of picoseconds to nanoseconds. Figure 27 shows the results of excite-probe measurements of TD2765 with a probe wavelength of 670 nm and three different excitation wavelengths. Exciting at 710 nm, (curve 1), no ESA is observed as verified by the full recovery of the probe signal within the pulse temporal length. At 700 nm, (curve 2), excite–probe measurements show a small fraction of ESA (signal lasting after the pulse), indicating mostly 2PA evidenced by a recovery of 94% of the normalized transmittance. Significant ESA is observed with an excitation wavelength of 690 nm in (curve 3). At 690 nm, the linear absorption cross-section is 1.6 x10^{-18} cm^2, almost three orders of magnitude smaller than the peak absorption cross-section, yet there is significant ESA. If the ESA was not accounted for in these measurements, it would have appeared that we measured a

2PA cross-section in excess of 35,000 GM, and the errors would probably be significantly larger even closer to the absorption edge. Analysis of the excite-probe data allows us to determine the relative contribution of ESA and 2PA and correct the Z-scan data to give the 2PA spectrum shown in Fig 26.

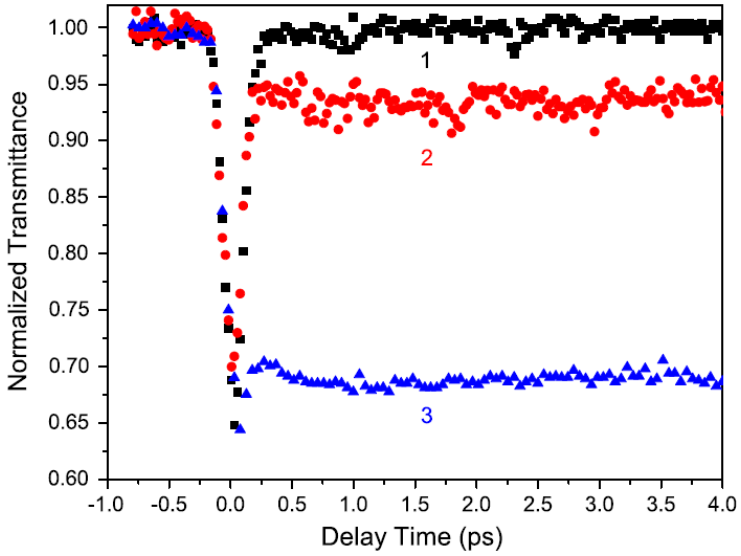

Figure 27. Normalized transmittance of TD2765 as a function of probe temporal delay with a probe wavelength of 670 nm and 3 different input excitation wavelengths getting closer to the linear absorption edge from (1) 710 nm, (2) 700 nm to (3) 690 nm for the tetraone molecule. The absorption peaks at 625 nm as shown in Fig. 26. This shows how resonant excitation of excited states grows to nearly dominate the absorption as the wavelength is reduced. From Ref. [83].

To measure the ESA spectrum shown in Fig. 28, a femtosecond excitation near the linear absorption resonance is used along with a white light continuum (WLC) probe. A description of this technique can be found in Refs. [53, 58] and is discussed in Sec. 3.2.2.

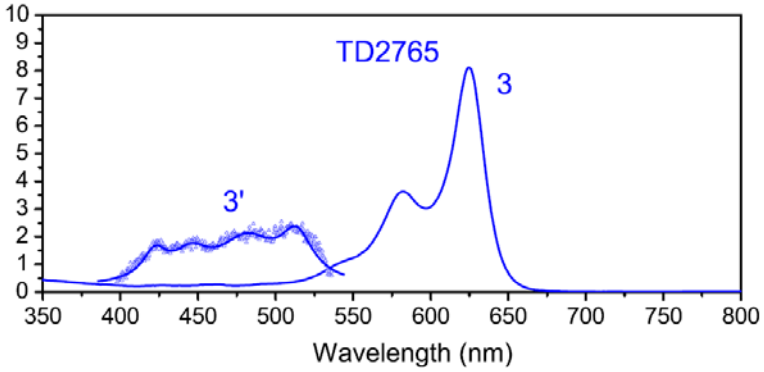

Figure 28. Absorption cross-section for TD 2765 (3), and the corresponding excited-state absorption spectrum 3'.

5. OTHER METHODS:

In this chapter we have discussed many methods that are used in nonlinear optical materials characterization along with other selected techniques. There are several other methods not discussed. Here we mention a few of these and give some references for further investigation. Thermal lensing from 2PA [84-86]

A. Related techniques to photothermal lensing [87, 88] are:
    a. Photothermal displacement [89]
    b. Photothermal beam deflection [90]
    c. Photoacoustic (optoacoustic) detection [91-94]
    d. Thermal calorimetry of 2PA [95]
    e. Photothermal interferometry [96]

B. Beam deflection.[97] This is a new excite-probe method that that allows a direct measurement of ultrafast or cumulative nonlinear refraction and nonlinear absorption to be measured with a demonstrated sensitivity to nonlinear phase distortion of $\lambda/20{,}000$.[70]

C. two-photon-induced phosphorescence to visualize singlet oxygen concentration [98]

D. Lifetime imaging to differentiate phosphorescence from fluorescence [99]

E. Multiphoton Ionization Spectroscopy [100-102]

6. CONCLUSION:

There are many different experimental methodologies for measuring nonlinear absorption. The associated nonlinear refraction can often lead to problems in unambiguously determining the nonlinear loss; thus it can be useful to simultaneously determine the nonlinear refraction. This can also be valuable for determining the underlying physical process or processes which can often be difficult. Parametric studies of the wavelength dependence, temporal dependence and sometimes the optical geometry dependence can also be important. The variety of nonlinear processes occurring in different materials is rich and complicated, and it is rarely the case that a single measurement at a single wavelength with a single pulsewidth can determine the physics involved in a nonlinear interaction. Modern nonlinear spectroscopic techniques are essential. Ultrafast nonlinearities often require femtosecond resolution to unambiguously determine their sign and magnitude. Longer pulses display other effects such as excited-state absorption and refraction which can even dominate the nonlinear response. The nonlinearities occurring in organic materials mimic the nonlinearities in semiconductors where free-carrier effects take the place of excited-state effects. However, unlike in semiconductors where the band structure determines the response, the individual molecular levels in organics can be engineered allowing the nonlinear

response to be altered. However, the magnitudes of the nonlinearities are still not as large as is needed for many of the applications including all-optical switching and optical limiting.

7. ACKNOWLEDGEMENTS:

We would like to thank the many former students and postdocs who worked on several of the methods and materials presented in this chapter as well as our current students. Special thanks go to our former student Joel Hales who provided data on some of the materials he studied after leaving CREOL. We also thank Mykhailo Bondar for proofreading the manuscript. We acknowledge the many sponsors of our research with recent thanks to the Air Force Office of Scientific Research (AFOSR) (FA9550-10-1-0558), and the National Science Foundation (NSF) (ECCS-1202471, ECCS-1229563).

[1] A. Penzkofer, W. Falkenstein, and W. Kaiser, "2-Photon Spectroscopy Using Picosecond Light Continua," *Applied Physics Letters,* vol. 28, pp. 319-321, 1976.
[2] B. H. Cumpston, S. P. Ananthavel, S. Barlow, D. L. Dyer, J. E. Ehrlich, L. L. Erskine*, et al.*, "Two-photon polymerization initiators for three-dimensional optical data storage and microfabrication," *Nature,* vol. 398, pp. 51-54, Mar 1999.
[3] A. E. Kaplan, "External self-focusing of light by a nonlinear layer," *Radiophys. Quantum Electron.,* vol. 12, p. 692—696, 1969.
[4] E. W. Van Stryland and L. L. Chase, "Two Photon Absorption: inorganic materials," in *Handbook of Laser Science and Technology; supplement 2: Optical Materials, section 8*. vol. Handbook of Laser Science and Technology; supplement 2: Optical Materials, section 8, M. Weber, Ed., ed: CRC Press, 1994, pp. 299-328.
[5] L. L. Chase and E. W. Van Stryland, "Nonlinear Refractive Index: inorganic materials," in *Handbook of Laser Science and Technology; supplement 2: Optical Materials, section 8*, M. Weber, Ed., ed: CRC Press, 1994, pp. 269-288.
[6] A. F. Garito and M. G. Kuzyk, "Two-Photon Absorption: Organic Materials," in *Handbook of Laser Science and Technology; supplement 2: Optical Materials*, M. Weber, Ed., ed: CRC Press, 1994, pp. 329-333.
[7] A. F. Garito and M. G. Kuzyk, "Nonnlinear Refractive Index: Organic Materials," in *Handbook of Laser Science and Technology; supplement 2: Optical Materials*, M. Weber, Ed., ed: CRC Press, 1994, pp. 289-298.
[8] J. A. Armstrong, N. Bloembergen, J. Ducuing, and T. P. S. Pershan, "Interactions between Light Waves in a Nonlinear Dielectric," *Phys. Rev.,* vol. 127, pp. 1918 – 1939, 1962.
[9] D. C. Hutchings, M. Sheik-Bahae, D. J. Hagan, and E. W. Van Stryland, "Kramers-Krönig relations in nonlinear optics," *Optical and Quantum Electronics,* vol. 24, pp. 1-30, 1992 1992.
[10] D. D. Smith, Y. Yoon, R. W. Boyd, J. K. Campbell, L. A. Baker, R. Crooks*, et al.*, "Z-scan measurement of the nonlinear absorption of a thin gold film," *J. of Appl. Phys.,* vol. 86, pp. 6200-6205, 1999.
[11] D. I. Kovsh, S. Yang, D. J. Hagan, and E. W. Van Stryland, "Nonlinear Optical Beam Propagation for Optical Limiting," *Applied Optics,* vol. 38, pp. 5168-5180, 1999.
[12] M. Göppert-Mayer, "Uber Elementarakte Mit Zwei Quantensprungen," *Ann. Phys.,* vol. 401, pp. 273-294, 1931.
[13] P. N. Prasad and D. J. Williams, *Introduction to nonlinear optical effects in molecules and polymers*. New York: Wiley, 1991.
[14] F. J. Aranda, D. V. G. L. N. Rao, J. F. Roach, and P. Tayebati, "Third-order nonlinear optical interactions of C60 and C70," *J. Appl. Phys.,* vol. 73, pp. 7949-7951, 1993.
[15] T. H. Wei, D. J. Hagan, M. J. Sence, E. W. Van Stryland, J. W. Perry, and D. R. Coulter, "Direct Measurements of Nonlinear Absorption and Refraction in Solutions of Phthalocyanines," *Applied Physics,* vol. B54, pp. 46-51, 1992.
[16] T. Xia, D. Hagan, A. Dogariu, A. Said, and E. W. Van Stryland, "Optimization of Optical Limiting Devices Based on Excited-State Absorption," *Applied Optics,* vol. 36, pp. 4110-4122, 1997.
[17] P. A. Miles, "Bottleneck optical limiters: the optimal use of excited-state absorbers," *Appl. Opt.,* vol. 33, pp. 6965–6979, 1994.
[18] R. L. Sutherland, M. C. Brant, J. Heinrichs, J. E. Rogers, J. E. Slagle, D. G. McLean*, et al.*, "Excited-state characterization and effective three-photon absorption model of two-photon-induced excited state absorption in organic push-pull charge-transfer chromophores," *J. Opt. Soc. Am. B-Opt. Phys.,* vol. 22, pp. 1939-1948, 2005.

[19] M. Rumi and J. W. Perry, "Two-photon absorption: an overview of measurements and principles," *Advances in Optics and Photonics,* vol. 2, pp. 451–518, 2010.
[20] J. H. Bechtel and W. L. Smith, "Two-photon absorption in semiconductors with picosecond laser pulses," *Phys. Rev.,* vol. B 13, 1976.
[21] E. W. Van Stryland, M. A. Woodall, H. Vanherzeele, and M. J. Soileau, "Energy band-gap dependence of two-photon absorption," *Optics Letters,* vol. 10, pp. 490-492, 1985.
[22] E. W. Van Stryland, M. Sheik-Bahae, A. A. Said, and D. J. Hagan, "Characterization of Nonlinear Optical Absorption and Refraction," *Journal of Progress in Crystal Growth and Characterization,* vol. 27, pp. 279-311, 1993.
[23] S.-H. Chi, J. M. Hales, M. Cozzuol, C. Ochoa, M. Fitzpatrick, and J. W. Perry, "Conjugated polymer-fullerene blend with strong optical limiting in the near-infrared," *Optics Express,* vol. 17, pp. 22062-72, 2009.
[24] E. W. Van Stryland, M. Sheik-Bahae, A. A. Said, D. J. Hagan, and M. J. Soileau, "Characterization of Nonlinear Optical Materials," *SPIE,* vol. 2114, pp. 444-468 1994.
[25] M. Sheik-Bahae, A. A. Said, and E. W. Van Stryland, "High Sensitivity, Single Beam n2 Measurements," *Opt. Lett.,* vol. 14, pp. 955-957 1989.
[26] M. Sheik-Bahae, A. A. Said, T. H. Wei, D. J. Hagan, and E. W. Van Stryland, "Sensitive Measurement of Optical Nonlinearities Using a Single Beam," *IEEE Journal of Quantum Electronics,* vol. 26, pp. 760-769, 1990.
[27] H. Ma, A. S. L. Gomes, and C. B. Dearaujo, "Measurements of Nondegenerate Optical Nonlinearity Using a 2-Color Single Beam Method," *Applied Physics Letters,* vol. 59, pp. 2666-2668, 1991.
[28] M. R. Ferdinandus, M. Reichert, T. R. Ensley, H. Hu, D. A. Fishman, S. Webster*, et al.*, "Dual-arm Z-scan technique to extract dilute solute nonlinearities from solution measurements," *Optical Materials Express,* vol. 2, pp. 1776-1790, 2012.
[29] T. Xia, D. J. Hagan, M. Sheik-Bahae, and E. W. Van Stryland, "Eclipsing Z-Scan Measurement of (lambda/10^4) Wavefront Distortion," *Opt. Lett.,* vol. 19, pp. 317-319, 1994.
[30] E. W. Van Stryland, M. Sheik-Bahae, T. Xia, C. Wamsley, Z. Wang, A. A. Said*, et al.*, "Z-scan and EZ-scan Measurements of Optical Nonlinearities," *International Journal of Nonlinear Optical Physics, IJNOP,* vol. 3, pp. 489-500, 1994.
[31] D. Weaire, B. S. Wherrett, D. A. B. Miller, and S. D. Smith, "Effect of low-power nonlinear refraction on laser-beam propagation in InSb," *Optics Letters,* vol. 4, pp. 331-333, 1979.
[32] W. Zhao, J. H. Kim, and P. Palffy-Muhoray, "Z-scan measurements on liquid crystals using Top-Hat beams," *Applied Physics Letters,* vol. 65, pp. 673–675, 1994.
[33] W. Zhao and P. Pallf-Muhory, "Z-scan technique using top-hat beams," *Appl. Phys. Lett.,* vol. 63, pp. 1613-1615, 1993.
[34] V. P. Kozich, A. Marcano, F. Hernandez, and J. Castillo, "Dual-beam time-resolved Z-scan in liquids to study heating due to linear and nonlinear light absorption," *Applied Spectroscopy,* vol. 48, pp. 1506-1512, 1994.
[35] J. Wang, M. Sheik-Bahae, A. A. Said, D. J. Hagan, and E. W. Van Stryland, "Time-Resolved Z-scan Measurements of Optical Nonlinearities " *JOSA* vol. B 11, pp. 1009-1017, 1994.
[36] J. Yang, X. Wu, M. Shi, Z. Li, Y. Yang, and Y. Son, "Sensitivity enhancement for measurement of nonlinear refraction using top-hat beams," *Appl. Phys. B,* vol. 110, pp. 591–594, 2013.
[37] T. Ensley, H. Hu, A. Ernst, C. Fuentes-Hernandez, A. Dindar, B. Kippelen*, et al.*, "Nonlinear Refraction Measurments of Thin Films by the Dual-Arm Z-scan Method," in *OSA Topical Conference, Nonlinear Optics*, Kohala Coast, Fairmont Hotel, Hawaii, 2013, p. talk NTu1B.4.

[38] A. A. Said, D. J. Hagan, E. W. Van Stryland, B. A. Reinhardt, P. Roderer , and A. G. Dillard, "Third and Fifth Order Optical Nonlinearities in Organic Materials," *Chem. Phys. Lett.,* vol. 228, pp. 646-650 1994.
[39] M. Balu, J. Hales, D. J. Hagan, and E. W. Van Stryland, "White-light continuum Z-scan technique for nonlinear materials characterization," *Optics Express,* vol. 12, pp. 3820-3826, Aug 2004.
[40] M. Balu, L. A. Padilha, D. J. Hagan, E. W. Van Stryland, S. Yao, K. Belfield*, et al.*, "Broadband Z-scan characterization using a high-spectral-irradiance, high-quality supercontinuum," *Journal of the Optical Society of America B-Optical Physics,* vol. 25, pp. 159-165, 2008.
[41] M. Balu, L. A. Padilha, D. J. Hagan, E. W. Van Stryland, S. Yao, K. Belfield*, et al.*, "Broadband Z-scan characterization using a high-spectral-irradiance, high-quality supercontinuum (vol 25, pg 159, 2008) erratum," *Journal of the Optical Society of America B-Optical Physics,* vol. 26, pp. 1663-1663, 2009.
[42] J. JChung, S. J. Zheng, T. Odani, L. Beverina, J. Fu, L. A. Padilha*, et al.*, "Extended Squaraine Dyes with Large Two-Photon Absorption Cross-Sections," *J. Am. Chem. Soc.,* vol. 128, pp. 14444-14445, 2006.
[43] M. Balu, J. M. Hales, D. J. Hagan, and E. W. Van Stryland, "Dispersion of nonlinear refraction and two-photon absorption using a white-light continuum Z-scan," *Optics Express,* vol. 13, pp. 3594-3599, 2005.
[44] P. B. Corkum, C. Rolland, and T. Srinivasanrao, "Supercontinuum Generation in Gases," *Physical Review Letters,* vol. 57, pp. 2268-2271, 1986.
[45] E. W. Van Stryland and M. Sheik-Bahae, "Z-Scan," in *Characterization Techniques and Tabulations for Organic Nonlinear Optical Materials*, M. Kuzyk and C. Dirk, Eds., ed: Marcel Decker, 1998, pp. 655-692.
[46] E. W. Van Stryland and D. J. Hagan, "Measuring Nonlinear Refraction and Its Dispersion via Propagation," in *Self-focusing: Past and Present*. vol. 114, R. Boyd, S. Lukishova, and R. Shen, Eds., ed: Springer Verlag, 2009, pp. 573-591.
[47] M. Sheik-Bahae, J. Wang, R. DeSalvo, D. J. Hagan, and E. W. Van Stryland, "Measurement of nondegenerate nonlinearities using a two-color Z scan," *Optics Letters,* vol. 17, pp. 258-260, 1992.
[48] S. Cherukulappurath, G. Boudebs, and A. Monteil, "4f coherent imager system and its application to nonlinear optical measurements," *J. Opt. Soc. Am. B,* vol. 21, pp. 273-279, 2004.
[49] *Picosecond Phenomena*: Springer-Verlag, 1978.
[50] R. S. Lepkowicz, O. V. Przhonska, J. M. Hales, D. J. Hagan, E. W. Van Stryland, M. V. Bondar*, et al.*, "Excited-state absorption dynamics in polymethine dyes detected by polarization-resolved pump-probe measurements," *Chemical Physics,* vol. 286, pp. 277-291, 2003.
[51] D. Peceli, H. H. Hu, D. A. Fishman, S. Webster, O. V. Przhonska, V. V. Kurdyukov*, et al.*, "Enhanced Intersystem Crossing Rate in Polymethine-Like Molecules: Sulfur-Containing Squaraines versus Oxygen-Containing Analogues," *Journal of Physical Chemistry A,* vol. 117, pp. 2333-2346, Mar 21 2013.
[52] D. Peceli, S. Webster, D. A. Fishman, C. M. Cirloganu, H. Hu, O. V. Przhonska*, et al.*, "Optimization of the Double Pump–Probe Technique: Decoupling the Triplet Yield and Cross Section," *J. Phys. Chem. A,* vol. 116, pp. 4833-4841, 2012.
[53] R. Negres, O. Przhonska, D. Hagan, E. Van Stryland, M. Bondar, Y. Slominsky*, et al.*, "The Nature of Excited-State Absorption in Polmethine and Squarylium Molecules," *IEEE Journal on Selected Topics in Quantum Electronics,* vol. 7, pp. 849-863, 2001.

[54] J. M. Hales, M. Cozzuol, T. E. O. Screen, H. L. Anderson, and J. W. Perry, "Metalloporphyrin polymer with temporally agile, broadband nonlinear absorption for ptical limiting in the near infrared," *Optics Express,* vol. 17, pp. 18478-18488, 2009.
[55] R. A. Negres, J. M. Hales, A. K. Kobyakov, D. J. Hagan, and E. W. Van Stryland, "Experiment and Analysis of Two-Photon Absorption Spectroscopy Using a White-Light Continuum Probe," *IEEE Jour. Quantum. Elect.,* vol. 38, pp. 1205-1216, 2002.
[56] R. A. Negres, J. M. Hales, A. K. Kobyakov, D. J. Hagan, and E. W. Van Stryland, "Experiment and Analysis of Two-Photon Spectroscopy and Analysis with a White-Light Continuum Probe, erratum," *IEEE Journ. Quant. Elect. ,* vol. 39, p. 392, 2003.
[57] R. Negres, J. M. Hales, A. Kobyakov, D. Hagan, and E. W. Van Stryland, "Two-Photon Spectroscopy and Analysis with a White-Light Continuum Probe," *Optics Letters,* vol. 27, pp. 270-272, 2002.
[58] R. S. Lepkowicz, O. V. Przhonska, J. M. Hales, J. Fu, D. J. Hagan, E. W. Van Stryland*, et al.*, "Nature of the Electronic Transitions in Thiacarbocyanines with a Long Polymethine Chain," *Chem. Phys.,* vol. 305, pp. 259-270, 2004.
[59] Yamaguchi and H. Hamaguchi, "Convenient method of measuring the chirp structure of femtosecond white-light continuum pulses," *Appl. Spectroscopy,* vol. 49, pp. 1513–1515, 1995.
[60] M. Sheik-Bahae, D. C. Hutchings, D. J. Hagan, and E. W. Van Stryland, "Dispersion of Bound Electronic Nonlinear Refraction in Solids," *IEEE Journal of Quantum Electronics,* vol. 27, pp. 1296-1309, 1991.
[61] F. Bassani and S. Scandolo, "Dispersion relations and sum rules in nonlinear optics," *Phys. Rev. B,* vol. 44, pp. 8446-8453 1991.
[62] I. Kang, T. Krauss, and F. Wise, "Sensitive measurement of nonlinear refraction and two-photon absorption by spectrally resolved two-beam coupling," *Opt. Lett.,* vol. 22, pp. 1077-1080 1997.
[63] J.-F. Ripoche, G. Grillon, B. Prade, M. France, E. Nibbering, R. Lange*, et al.*, "Determination of the time dependence of n2, in air"," *Opt. Commun.,* vol. 135, pp. 310-314 1997.
[64] R. K. Jain and M. B. Klein, "Degenerate four-wave-mixing in semiconductors," in *Optical Phase Conjugation*, R. A. Fisher, Ed., ed New York: Academic Press, 1983, pp. 307-455
[65] A. L. Smirl, T. F. Bogges, B. S. Wherrett, G. P. Perryman, and A. Miller, "Picosecond optically induced anisotropic state filling in semiconductors," *Phys. Rev. Lett.,* vol. 49, pp. 993-936 1982.
[66] M. Sheik-Bahae, J. Wang, E. J. Canto-Said, R. DeSalvo, D. J. Hagan, and E. W. Van Stryland, "Polarization Dependent Four-Wave Mixing and Two-Photon Coherence in Solids," *IEEE Journ. Quant. Electron.,* vol. 31, pp. 1270-1273, 1995.
[67] *Optical Phase Conjugation*: Academic Press, 1983.
[68] S. Y. Tseng, W. Cao, Y. H. Peng, J. M. Hales, S. H. Chi, J. W. Perry*, et al.*, "Measurement of complex Chi((3)) using degenerate four-wave mixing with an imaged 2-D phase grating," *Opt Express,* vol. 14, pp. 8737-8744, 2006.
[69] W. Cao, Y.-H. Peng, Y. Leng, C. H. Lee, W. N. Herman, and J. Goldhar, "Phase Scan Technique for Measuring Phase of Complex χ(3) of Nonlinear Polymer Thin Films," in *Organic Thin Films for Photonic Applications*, ed Washington, DC., 2010, pp. 139-157.
[70] M. Reichert, H. Hu, M. R. Ferdinandus, M. Seidel, P. Zhao, T. R. Ensley*, et al.*, "Temporal, spectral, and polarization dependence of the nonlinear optical response of carbon disulfide," *Optica,* vol. 1, pp. 436-445, 2014.
[71] W. Kaiser and C. G. B. Garrett, " Two-Photon Excitation in CaF_{2}: Eu^{2+}," *Phys Rev Lett,* vol. 7, pp. 229-231, 1961.
[72] P. A. Franken, A. E. Hill, C. W. Peters, and G. Weinreich, "Generation of Optical Harmonics," *Phys. Rev. Lett.,* vol. 7, pp. 118-119, 1961.

[73] C. Xu and W. W. Webb, "Measurement of Two-Photon Excitation Cross Sections of Molecular Fluorophores with Data from 690 to 1050 nm," *J. Opt. Soc. Am. B,* vol. 13, pp. 481-491, 1996.
[74] *Topics in Fluorescence Spectroscopy, Volume 5 Nonlinear and Two-Photon Induced Fluorescence* vol. 5. New York: Kluwer Academic Publishers, 2002.
[75] W. R. Zipfel, R. M. Williams, R. Christie, A. Y. Nikitin, B. T. Hyman, and W. W. Webb, "Live tissue intrinsic emission microscopy using multiphoton-excited native fluorescence and second harmonic generation," *Proc Natl Acad Sci U S A,* vol. 100, pp. 7075-80, 2003.
[76] W. R. Zipfel, R. M. Williams, and W. W. Webb, "Nonlinear Magic: Multiphoton Microscopy in the Biosciences," *Nat Biotech,* vol. 21, pp. 1369-1377, 2003.
[77] N. S. Makarov, M. Drobizhev, and A. Rebane, "Two-Photon Absorption Standards in the 550-1600 Nmexcitation Wavelength Range," *Opt. Express,* vol. 16, pp. 4029-4047, 2008.
[78] N. S. Makarov, J. Campo, J. M. Hales, and J. W. Perry, "Rapid, broadband two-photon-excited fluorescence spectroscopy and its application to red-emitting secondary reference compounds," *Optical Materials Express,* vol. 1, pp. 551-563, 2011.
[79] J. R. Lakowicz, *Principles of Fluorescence Spectroscopy: Third Edition*, 3rd ed.: Springer, 2006.
[80] P. R. Callis, "The Theory of Two-Photon-Induced Fluorescence Anisotropy," in *Topics in FLuorescewnce Spectroscopy, Volume 5 Nonlinear and Two-Photon Induced Fluorescence*. vol. 5, J. R. Lakowicz, Ed., ed New York: Kluwer Academic Publishers, 2002, pp. 1-42.
[81] J. Fu, O. V. Przhonska, L. A. Padilha, D. J. Hagan, E. W. Van Stryland, K. D. Belfield*, et al.*, "Two-photon anisotropy: analytical description and molecular modeling for symmetrical and asymmetrical organic dyes," *Chem. Phys.,* vol. 321, pp. 257–268 2006.
[82] J. Fu, L. A. Padilha, D. J. Hagan, E. W. Van Stryland, O. V. Przhonska, M. V. Bondar*, et al.*, "Experimental and theoretical approaches to understanding two-photon absorption spectra in polymethine and squaraine molecules," *J. Opt. Soc. Am. B,* vol. 24, pp. 67-76, 2007.
[83] S. Webster, J. Fu, L. A. Padilha, O. V. Przhonska, D. J. Hagan, E. W. Van Stryland*, et al.*, "Comparison of nonlinear absorption in three similar dyes: Polymethine, squaraine and tetraone," *Chemical Physics,* vol. 348, pp. 143-151, 2008.
[84] J. Castillo, V. P. Kozich, and A. O. Marcano, "Thermal lensing resulting from one- and two-photon absorption studied with a two-color time-resolved Z scan," *Optics Letters,* vol. 19, pp. 171-173, 1994.
[85] V. P. Kozich, A. O. Marcano , F. E. Hernández, and J. Castillo, "Use of Differential Thermal Lensing to Study Two-Photon Absorption in Solutions," *Applied Spectroscopy,* vol. 48, pp. 1419-1422, 1994.
[86] W. T. White III , M. A. Henesian, and M. Weber, "Photothermal-lensing measurements of two-photon absorption and two-photon-induced color centers in borosilicate glasses at 532 nm," *J. Opt. Soc. Am. B,* vol. 2, pp. 1402-1408 1985.
[87] A. Kurian, S. T. Lee, K. P. Unnikrishnan, D. Sajan, V. P. N. Nampoori, and C. P. G. Vallabhan, "Studies on Two-Photon Absorption of Aniline Using Thermal Lens Effect," *Journal of Nonlinear Optical Physics & Materials* vol. 9, pp. 75-80, 2003.
[88] H. L. Fang, T. L. Gustafson, and R. L. Swofford, "Two-photon absorption photothermal spectroscopy using a synchronously pumped picosecond dye laser. Thermal lensing spectra of naphthalene and diphenylbutadiene," *J. Chem. Phys.,* vol. 78, 1983.
[89] M. A. Olmstead and N. M. Amer, "A new probe of the optical properties of surfaces," *J. Vac. Sci. Technol. B,* vol. 1, pp. 751-753, 1983.
[90] W. B. Jackson, N. M. Amer, A. C. Boccara, and D. Fournier, "Photothermal deflection spectroscopy and detection," *Appl. Opt.,* vol. 20, pp. 1333-1344, 1981.

[91] J. Badoz and D. Fournier, Eds., *Photoacoustic and photothermal spectroscopy* Colloq. (C6)). J. Phys. (Paris), 1983.
[92] A. C. Tam, "Applications of photoacoustic sensing techniques," *Rev. Mod. Phys. ,* vol. 58, pp. 381-3, 1986.
[93] E. W. Van Stryland and M. A. Woodall, "Photoacoustic Measurement of Nonlinear Absorption in Solids," in *Laser Induced Damage in Optical Materials, Boulder Damage Symposium*, Boulder, CO, 1980, p. 50.
[94] J. A. Sell, Ed., *Photothermal Investigations of Solids and Fluids*. Academic Press, 1989.
[95] M. Bass, E. W. Van Stryland, and A. F. Stewart, "Laser calorimetric measurement of two-photon absorption," *Appl. Phys. Lett. ,* vol. 34, pp. 142-144 1979.
[96] E. A. McLean, L. Sica, and A. J. Glass, "Interferometric observation of absorption induced index change associated with thermal blooming," *Appl. Phys. Lett.,* vol. 13, pp. 369-371 1968.
[97] M. R. Ferdinandus, H. Hu, M. Reichert, D. J. Hagan, and E. W. Van Stryland, "Beam deflection measurement of time and polarization resolved ultrafast nonlinear refraction," *Optics Letters,* vol. 38, pp. 3518-3521, 2013.
[98] O. S. Finikova, A. Y. Lebedev, A. Aprelev, T. Troxler, F. Gao, C. Garnacho*, et al.*, "Oxygen Microscopy by Two-Photon-Excited Phosphorescence," *Chem. Phys. Chem.,* vol. 9, pp. 1673-1679, 2008.
[99] S. S. Howard, A. Straub, N. G. Horton, D. Kobat, and C. Xu, "Frequency-multiplexed in vivo multiphoton phosphorescence lifetime microscopy," *Nature Photonics,* vol. 7, pp. 33–37, 2013.
[100] S. Zhang, C. Lu, T. Jia, J. Qiu, and Z. Sun, "Resonance-enhanced multiphoton-ionization photoelectron spectroscopy by a rectangular amplitude modulation," *Phys. Rev. A,* vol. 87, 2013.
[101] P. M. Johnson, "Molecular multiphoton ionization spectroscopy", Philip M. Johnson," *Applied Optics,* vol. 19, pp. 3920-3925, 1980.
[102] J. B. Milan, W. J. Buma, and C. A. de Lange, "Two-photon resonance enhanced multiphoton ionization photoelectron spectroscopy of the SH (SD) radical below and above the lowest ionization threshold," *J. Chem. Phys.,* vol. 105, pp. 6688-6712, 1996.